Sharif University of Technology

Scientia Iranica

Transactions on Mechanical Engineering

https://scientiairanica.sharif.edu

Practical bifurcation analysis for the vibration's proficiency and their influences on gas turbine operations: Towards the digitization of their monitoring

Youcef Mahroug [a], Ahmed Hafaifa [b,c,*], Abdelhamid Iratni [d], Mouloud Guemana [b,e], Ilhami Colak [c]

a. Laboratory of Mechanics, Physics and Mathematical Modelling, University of Medea, 26000, Medea, Algeria.
b. Applied Automation and Industrial Diagnostics Laboratory, Faculty of Science and Technology, University of Djelfa 17000 DZ, Algeria.
c. Department of Electrical and Electronics Engineering, Faculty of Engineering and Natural Science, Istinye University, İstanbul, Turkey.
d. Faculty of Science and Technology, University of Bordj Bou Arreridj, 34030 DZ, Algeria.
e. Gas Turbine Joint Research Team, University of Djelfa, Djelfa 17000 DZ, Algeria.

* Corresponding author: a.hafaifa@univ-djelfa.dz (A. Hafaifa)

Received 13 July 2022; received in revised form 14 October 2023; accepted 13 March 2024

Keywords

Stability analysis;
Bifurcation indices;
Equilibrium equations;
Gas turbines;
Vibration reduction.

Abstract

The emergence of modern technology in the oil and gas sectors presents an opportunity to enhance productivity, minimize environmental impact and optimize the energy efficiency of these facilities, leading to increased economic benefits. In pursuit of sustainable development in gas-turbine operations, this study develops a mathematical model that is validated through experimental tests for monitoring the vibrations of an MS5002B gas turbine located in a gas compressor station. The primary objective is to determine the bifurcation indices, ensuring the continuous stability of the studied turbine's operating state while monitoring its vibrations in real-time. A comparison between the experimental and numerical results of the developed model is validated against real operating data, enabling predictions of the complex dynamic behaviors within the bearing-rotor system of the examined turbine. Robustness tests, based on real-time operating data, are conducted to analyze the impacts of undesirable effects that may disrupt the turbine system, as depicted in the bifurcation diagram. This approach facilitates the monitoring of the dynamic behavior of vibratory phenomena in the examined turbine, allowing for the establishment of reliable diagnostic elements to ensure component stability and prevent unscheduled production shutdowns. Ultimately, this approach enhances energy efficiency while delivering environmental and economic improvements.

1. Introduction

In recent times, advancements in modern technologies and computing have provided reliable tools for enhancing the profitability and sustainability of industrial facilities. These innovations have the potential to improve both environmental and economic performance. Nevertheless, the monitoring of gas turbines in the oil and gas sector remains a significant challenge. The primary concern lies in mitigating the adverse effects resulting from sequences of turbine start-ups, optimizing yields, enhancing production performance, and preventing unforeseen failures.

To address this issue, this study proposes an original approach centered on the analysis of vibratory phenomena bifurcation within the bearing-rotor system of the MS5002B turbine, situated in a gas compression station. The objective is to ensure effective monitoring of this turbine, incorporating practical models characterizing the dynamic behaviors of vibration bifurcations that affect the examined turbine. This is achieved by integrating degradation evaluation indices, employing experimental tests based on turbine input/output data to predict real-time vibration cycles.

To cite this article:
Y. Mahroug, A. Hafaifa, A. Iratni, M. Guemana, I. Colak "Practical bifurcation analysis for the vibration's proficiency and their influences on gas turbine operations: Towards the digitization of their monitoring", *Scientia Iranica* (2025) **32**(6): 6990.
https://doi.org/10.24200/sci.2024.60787.6990.

To address the complexities of dynamic behavior in gas turbine systems subjected to high-power transmission and rotation, a monitoring approach based on various vibration bifurcations is implemented for the MS5002B turbine bearing-rotor system, taking into consideration the stability-to-efficiency ratio.

It is essential to recognize that rotating machines can encounter balance issues stemming from multiple sources of instability, particularly those caused by rotor-stator contact. Vibration dynamics can pose significant risks to rotating systems. Therefore, the rotational state must be considered when aligning the shaft to prevent bearing damage. Previous work in modern literature has been dedicated to the study of rotor stability and their responses at bifurcation limits. For example, Wang and Khonsari [1] conducted bifurcation analysis to evaluate the stiffness effects of a flexible rotor supported by plain bearings, leading to a dynamic characteristics model of the rotor-bearing system. In [2], the influence of oil temperature on the instability limit threshold of this rotor-bearing system was studied and validated by several experimental tests to evaluate the behavior of hydrodynamic plain bearings. Additionally, Chasalevris et al. [3] determined the additional harmonics affecting plain bearings using a magnetic geometry of these bearings, with experimental validation on 20% of the bearing radial clearance and 40% of other defects with critical speeds. Miraskari et al. [4] delved into the influence of nonlinear dynamics to determine the types of bifurcations affecting flexible rotors supported by plain bearings, facilitating the development of models for Hopf-type bifurcations. In [5], a numerical model of rotor-bearing system bearings was proposed by introducing disturbances to the Reynolds lubrication equation model, which allowed for the analysis of eigenvalues and the output of bifurcation directions of this rotor-bearing system. Anastasopoulos and Athanasios [6] studied the limit cycles of bifurcations in a rotor supported by plain bearings, enabling an analysis of the stability of the rotor-bearing system.

Furthermore, Noah and Sundararajan [7] investigated the importance of nonlinear effects on the dynamic behavior of rotating machines, especially fluid film bearings, conducting performance tests on a rotor system with multiple degrees of freedom. Mahroug et al. [8] studied the vibration behaviors of the bearings of a rotating machine, allowing the identification of defects using the ARMAX modeling structure. Ehrich [9] explored subcritical chaotic phenomena in a rotor, observing super-harmonic responses, which led to the analysis of bifurcation models obtained at the entrance and exit of different chaotic areas.

Several studies have examined monitoring and diagnostic systems for gas turbine failures, proposing various approaches. Wu [10] introduced an approach to analyze the dynamic performance of a gas turbine shaft, using artificial neural networks to enhance energy efficiency through in depth optimization of the turbine's performance analysis. Ju et al. [11] suggested a strategy of nonlinear feedback control for the vibration of the main transmission system of the scraper conveyor using bifurcations, while estimating the influence of these bifurcations on the torsional instability of the transmission shaft. Li et al. [12] conducted a nonlinear dynamic study of a rotor-bearing system, considering the effects of misalignment faults and analyzing nonlinear dynamic behaviors supported by sliding bearings. Several other works have been undertaken, exploring different bifurcation analyses of vibration and fault-tolerant control to monitor gas turbines in their design and implementation, as carried out by Hafaifa et al. [13], Djeddi et al. [14], Mohamadi et al. [15], Avramov and Malyshev [16], Avramov and Raimberdiyev [17], Aghayari et al. [18], Ma et al. [19], Noiray and Schuermans [20], and Mao et al. [21].

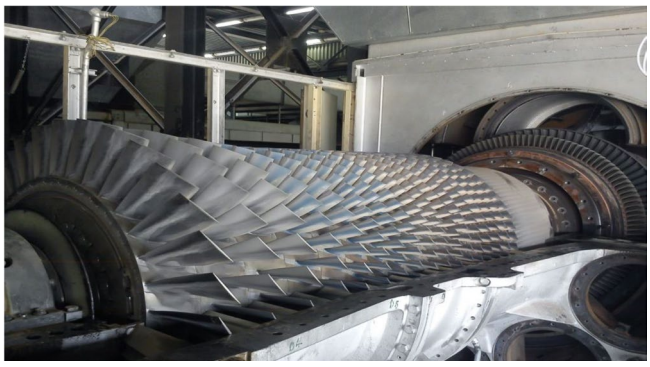

Figure 1. MS5002B gas turbine installed in the CS2/TFT gas compressor station in southeastern.

Understanding the dynamic behavior of turbines is vital to account for undesirable effects on their operation and to enhance efficiency and yield by managing the complex nonlinearities of vibratory behavior under severe conditions, such as high rotational speed, temperature, and pressure. To achieve this, gas turbine operators must design robust and reliable monitoring systems to detect anomalies and their potentially dangerous developments in turbine components. In this context, this study proposes a bifurcation analysis approach based on modeling the MS5002B turbine rotor-bearing system, aiming to extend its operational life while reducing maintenance costs. This approach involves analyzing spectra of frequency, phase portraits, and Poincaré maps to describe the stability changes in the curves of solutions depicted in various bifurcation diagrams, all based on real-time measurements.

2. The MS5002B gas turbine

In pursuit of enhancing the energy efficiency of gas turbines used in the natural gas transportation sector, along with the integration of modern monitoring practices to ensure their continuous availability while preventing sudden failures, our focus in this study centers on the MS5002B gas turbine, as depicted in Figure 1, with its specifications provided in Table 1. This specific turbine is situated at the CS2/TFT gas compressor station, operated by SONATRACH, located approximately 1400 km southeast of Algeria and 540 km from the Wilaya of ILLIZI in southern Algeria. The MS5002B turbine is engineered to deliver substantial power under optimal operating conditions, effectively driving a centrifugal gas compressor. Notably, it comprises two mechanically independent rotors, as illustrated in Figure 2.

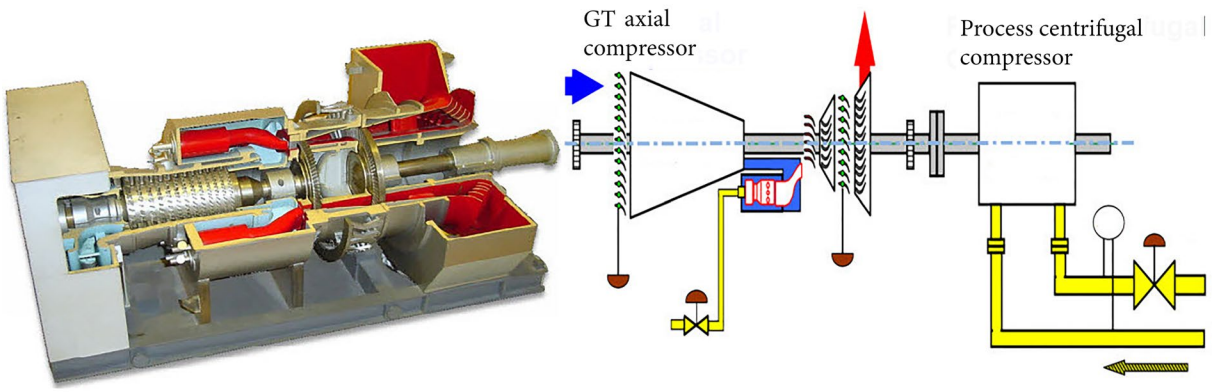

Figure 2. Operational structure of the MS5002B gas turbine.

Table 1. Specifications of the MS5002B gas turbine.

Parameters	Values
Cycle	Simple
Pressure ratio	6 – 8
Exhaust temperature	963 °F
Exhaust flow	274.1 Ibs/sec
Number of turbine stages	02
Rated power	38000 HP
Heat rate	8816 btu/hp-h
Turbine efficiency	28.8 %
Shaft speed	5100 rpm HP and 4903 rpm LP

The first rotor operates at speeds of up to 5100 rpm and is responsible for driving the axial compressor, featuring sixteen compression stages of the high-pressure HP turbine. Its primary function is to compress the air, which must be supplied to the combustion chambers under pressure. The second rotor is that of the low-pressure LP turbine, which is coupled mechanically to the centrifugal compressor.

To meet the goals concerning the analysis of vibratory dynamics, we begin with the processing of information and data to detect vibration anomalies, as detailed in the following section. This process initiates with the modeling of the bearing-rotor system of the examined MS5002B turbine. Subsequently, bifurcation indicators are employed to pinpoint the stability endpoints, providing reliable solutions for monitoring instability phenomena. This approach is critical for preventing any degradation of the turbine, ensuring stable and secure operation while aligning with the desired operation parameters to extend its operational lifespan. The method facilitates the early detection of malfunctions and enables continuous monitoring to plan maintenance interventions. These interventions encompass leveraging a range of failure detection techniques and modern supervision methods to develop intelligent monitoring tools tailored to the specific requirements of the examined turbine.

Multiple data series are collected through direct measurements of the rotating components of the machine shafts using various sensors positioned on these shafts. These sensors redundantly measure shaft movements and trigger immediate alarms in the event of a malfunction or a violation of vibration detection thresholds, as outlined in Table 2.

Table 2. Vibrations alarms in the MS5002B gas turbine.

	Alarm level	Danger level
Bearing N°1	12.7 mm/s	25.4 mm/s
Bearing N°4	12.7 mm/s	25.4 mm/s

Table 3. Type of MS5002B turbine bearings.

Bearing N°	Class	Type
1	Journal	Elliptical
	Thrust (active side)	Tilting pad (self-equalizing)
	Thrust (inactive side)	Tapered land
2	Journal	Elliptical
3	Journal	Tilting pad
4	Journal	Tilting pad
	Thrust (active side)	Tilting pad (self-equalizing)
	Thrust (inactive side)	Tilting pad (non-equalizing)

2.1. Modeling of MS5002B turbine bearing-rotor system

Monitoring the vibrations of gas turbines involves tracking their behavior based on operational parameters. This type of monitoring is straightforward when dealing with simple vibratory signals. However, it becomes complex and impractical when these signals have diverse origins and dynamics, a common occurrence with rotating machines. These machines produce vibrations that manifest simultaneously in numerous locations across various elements, each exhibiting different types of vibrations. In this context, the bearing-rotor system, illustrated in Figure 3, is used to model the dynamic behavior of vibrations in the MS5002B turbine. This system comprises two journal bearings with oil film, one for the axial compressor and one for the turbine.

The structure of the MS5002B turbine rotor-bearing system, examined in this study, comprises two plain bearings (journal bearings) for supporting the HP and LP rotors, along with a thrust bearing, as outlined in Table 3. The thrust bearing serves to maintain the axial position of the rotor-stator and support the axial thrust loads transmitted by the rotor.

The analysis of the rotor-bearing system's behavior focuses on the radial vibrations of the high-pressure HP turbine rotor. This analysis helps determine the significant

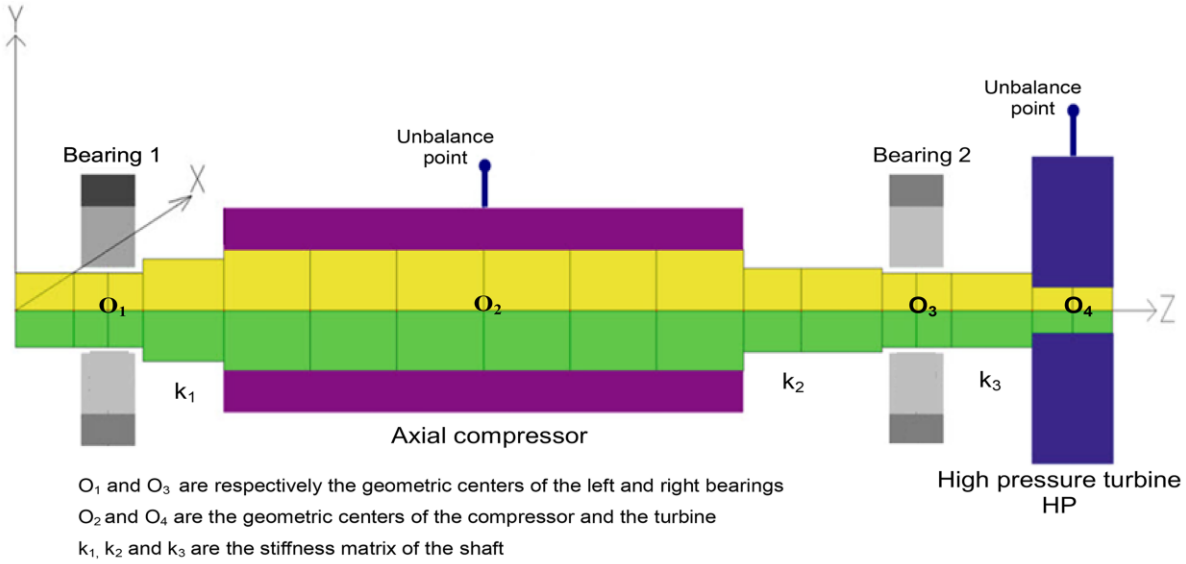

Figure 3. Structure of studied gas turbine rotor-bearing system.

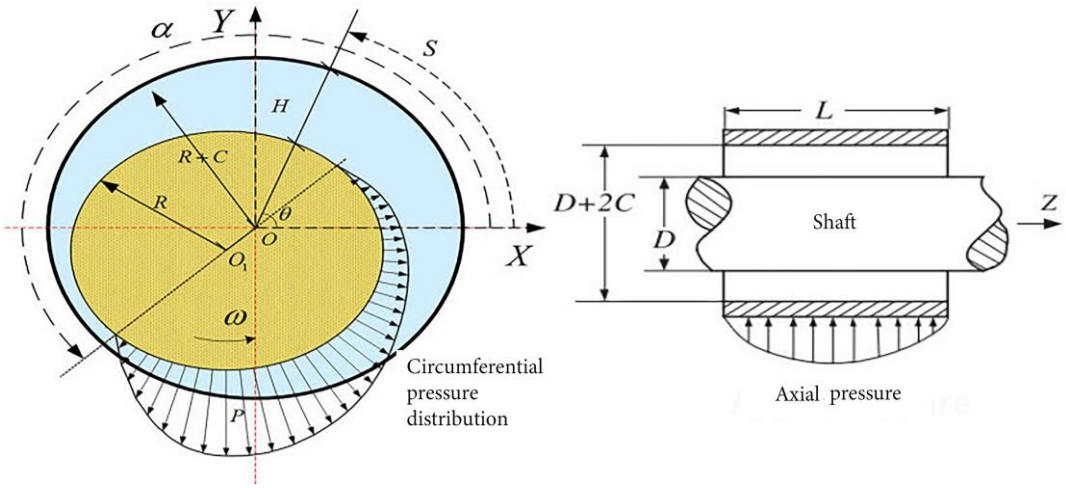

Figure 4. Representation of pressure distribution of the oil film.

impacts of these vibrations on the overall operation of the turbine. It also involves a thorough examination of the behaviors of the plain bearings, given their critical role in managing and mitigating the radial vibrations of the HP rotor. It's important to note that these bearings themselves can be a source of radial vibrations, particularly those generated within the HP rotor. These vibrations can have significant consequences on the efficiency, durability, and overall performance of the turbine. They can lead to premature wear of components and compromise system stability, resulting in substantial maintenance costs.

In practice, vibration monitoring is a highly intricate task that necessitates robust and reliable turbine operating data. This data ensures the effective protection of the rotating machine by automatically triggering shutdown or generating alarms before severe damage occurs to its components. The vibrations recorded in the examined MS5002B turbine bearing-rotor system can be attributed to various forces and non-linear effects of the oil film. These effects occur when the fluid film is generated by the relative movement of two surfaces, ensuring no contact between the shaft and the bearings. This arrangement is characteristic of hydrodynamic bearings, which serve as supporting elements for turbine rotors. They guide rotating shafts, boasting a notably high load capacity, where shaft rotation generates viscous damping and rigidity within the bearing, as depicted in Figure 4.

The nonlinear model of the hydrodynamic forces under the hypothesis of the short bearing, i.e., the ratio of its length to its diameter (L/D) has a low value ≤0.7, where the calculations of this type of bearing are based on the made that the circumferential pressure gradient is negligible, using the Reynolds equation the model of the hydrodynamic forces in the Cartesian frame of reference is given as follows [13, 22-24]:

$$\left(\frac{R}{L}\right)^2 \frac{\partial}{\partial z}\left(h^3 \frac{\partial p}{\partial z}\right) = -2\left(y' \sin\theta + x' \cos\theta\right) - y\cos\theta + x\sin\theta, \quad (1)$$

where R and L are respectively are the radius and the length of the bearing, $z = \frac{Z}{L}$ is the dimensionless axial displacement with; $-\frac{1}{2} \le z \le +\frac{1}{2}$, $p = \frac{P}{6\mu w\left(\frac{R}{C_b}\right)}$ is the dimensionless

pressure of the oil film with C_b is the radial clearance of the bearing, x and y are dimensionless horizontal and vertical displacements, $h = \frac{H}{C_b}$ is the dimensionless thickness of the oil film with $h = 1 - x\cos\theta - y\sin\theta$.

Integrating the Reynolds Eq. (1) gives the dimensionless pressure distribution of the oil film as follows [25- 28]:

$$p = \frac{1}{2}\left[\frac{L}{D}\right]^2 \frac{(x-2y')\sin\theta - (y+2x')\cos\theta}{(1-x\cos\theta - y\sin\theta)^3}\left(4z^2-1\right). \tag{2}$$

As well as the total nonlinear forces of the oil film are calculated by the formulation given in following [13, 29-31]:

$$\begin{aligned} F_X &= -\left[6\mu\omega\left(\frac{R}{C_b}\right)^2 RL\right]\int_{\alpha}^{\alpha+\pi}\int_{-1/2}^{1/2} p\cos\theta dz d\theta \\ F_Y &= -\left[6\mu\omega\left(\frac{R}{C_b}\right)^2 RL\right]\int_{\alpha}^{\alpha+\pi}\int_{-1/2}^{1/2} p\sin\theta dz d\theta \end{aligned} \tag{3}$$

Substituting Eq. (2) into Eq. (3) gives the dimensionless equations of oil film forces expressed as follows [13, 28, 29, 32]:

$$\begin{cases} f_x = \dfrac{1}{\sigma}F_X \\ \quad = 2\displaystyle\int_{\alpha}^{\alpha+\pi} \frac{(x-2y')\sin\theta\cos\theta - (2x'+y)\cos^2\theta}{(1-x\cos\theta - y\sin\theta)^3} d\theta \\ f_y = \dfrac{1}{\sigma}F_Y \\ \quad = 2\displaystyle\int_{\alpha}^{\alpha+\pi} \frac{(x-2y')\sin^2\theta - (y+2x')\cos\theta\sin\theta}{(1-x\cos\theta - y\sin\theta)^3} d\theta \end{cases} \tag{4}$$

with :

$$\sigma = \mu\omega RL\left(\frac{R}{C_b}\right)^2\left(\frac{L}{2R}\right)^2. \tag{5}$$

The resulting calculation of integration of Eq. (4) is written as follows [13, 27]:

$$\begin{aligned} f_x &= 2(x-2y')I_3 - 2(y+2x')I_1, \\ f_y &= 2(x-2y')I_2 - 2(y+2x')I_2, \end{aligned} \tag{6}$$

with :

$$\begin{aligned} I_1(x,y,\alpha) &= \int_{\alpha}^{\alpha+\pi} \frac{\cos^2\theta}{(1-x\cos\theta - y\sin\theta)^3} d\theta, \\ I_2(x,y,\alpha) &= \int_{\alpha}^{\alpha+\pi} \frac{\sin^2\theta}{(1-x\cos\theta - y\sin\theta)^3} d\theta, \\ I_3(x,y,\alpha) &= \int_{\alpha}^{\alpha+\pi} \frac{\cos\theta\sin\theta}{(1-x\cos\theta - y\sin\theta)^3} d\theta. \end{aligned} \tag{7}$$

By introducing $T(x,y,\alpha) = \int_{\alpha}^{\alpha+\pi} g(x,y,z)d\theta$ with $g(x,y,z) = \frac{1}{1-x\cos\theta - y\sin\theta}$ and using Leibniz's integral rule, the variables I_1, I_2 and I_3 are calculated as follows [33,34]:

$$\begin{aligned} I_1 &= \frac{1}{2}\frac{\partial^2 T}{\partial x^2} + \frac{\partial g(\alpha)}{\partial x}\frac{\partial \alpha}{\partial x} - \frac{\partial g(\alpha+\pi)}{\partial x}\frac{\partial \alpha}{\partial x} + \frac{1}{2}g(\alpha)\frac{\partial^2\alpha}{\partial x^2} \\ &\quad + \frac{1}{2}g(\alpha+\pi)\frac{\partial^2\alpha}{\partial x^2}, \\ I_2 &= \frac{1}{2}\frac{\partial^2 T}{\partial y^2} + \frac{\partial g(\alpha)}{\partial y}\frac{\partial \alpha}{\partial y} - \frac{\partial g(\alpha+\pi)}{\partial y}\frac{\partial \alpha}{\partial y} + \frac{1}{2}g(\alpha)\frac{\partial^2\alpha}{\partial y^2} \\ &\quad + \frac{1}{2}g(\alpha+\pi)\frac{\partial^2\alpha}{\partial y^2}, \\ I_3 &= \frac{1}{2}\frac{\partial^2 T}{\partial x\partial y} - \frac{\partial g(\alpha+\pi)}{\partial x}\frac{\partial \alpha}{\partial y} + \frac{1}{2}\frac{\partial g(\alpha)}{\partial y}\frac{\partial \alpha}{\partial x} \\ &\quad - \frac{1}{2}\frac{\partial g(\alpha)}{\partial x}\frac{\partial \alpha}{\partial y} + \frac{1}{2}g(\alpha)\frac{\partial^2\alpha}{\partial x\partial y} - \frac{1}{2}g(\alpha+\pi)\frac{\partial^2\alpha}{\partial x\partial y}. \end{aligned} \tag{8}$$

Then, substituting Eq. (8) into Eq. (6), the forces f_x and f_y are expressed as follows [35-38]:

$$\begin{bmatrix} f_x \\ f_y \end{bmatrix} = -\frac{\left[(x-2y')^2 + (y+2x')^2\right]^{\frac{1}{2}}}{1-x^2-y^2} \times \begin{bmatrix} 3xV(x,y,\alpha) - T(x,y,\alpha)\sin\alpha - 2S(x,y,\alpha)\cos\alpha \\ 3yV(x,y,\alpha) + T(x,y,\alpha)\cos\alpha - 2S(x,y,\alpha)\sin\alpha \end{bmatrix}, \tag{9}$$

where:

$$\begin{cases} V(x,y,\alpha) = \dfrac{2 + (y\cos\alpha - x\sin\alpha)T(x,y,\alpha)}{1-y^2-x^2} \\ S(x,y,\alpha) = \dfrac{y\sin\alpha + x\cos\alpha}{1-(y\sin\alpha + x\cos\alpha)^2} \\ T(x,y,\alpha) = \dfrac{2}{\left(1-y^2-x^2\right)^{\frac{1}{2}}}\left[\dfrac{\pi}{2} + arctg\dfrac{y\cos\alpha - x\sin\alpha}{\left(1-x^2-y^2\right)^{\frac{1}{2}}}\right] \\ \alpha = arctg\dfrac{2x'+y}{x-2y'} - \dfrac{\pi}{2}sign(2x'+y) - \dfrac{\pi}{2}sign\left(\dfrac{y+2x'}{x-2y'}\right) \end{cases} \tag{10}$$

With σ is the Sommerfeld number, μ is the dynamic viscosity, while f_x and f_y are the dimensionless nonlinear forces of the oil film.

2.2. *Governing equations of the bearing-rotor system of the MS5002B turbine*

The dynamic equations of a bearing-rotor system of a gas turbine are established by neglecting the shear strain and the gyroscopic torque to demonstrate the effect of the oil film force as follows:

$$\begin{aligned} &m_1\ddot{X}_1 + c\dot{X}_1 + k_1(X_1 - X_2) = F_{X_1} \\ &m_1\ddot{Y}_1 + c\dot{Y}_1 + k_1(Y_1 - Y_2) = F_{Y_1} - m_1 g \\ &m_2\ddot{X}_2 + c\dot{X}_2 + k_1(X_2 - X_1) + k_2(X_2 - X_3) = m_2 r\omega^2\cos(\omega t) \\ &m_2\ddot{Y}_2 + c\dot{Y}_2 + k_1(Y_2 - Y_1) + k_2(Y_2 - Y_3) = m_2 r\omega^2\sin(\omega t) - m_2 g \\ &m_3\ddot{X}_3 + c\dot{X}_3 + k_2(X_3 - X_2) + k_3(X_3 - X_4) = F_{X_3} \\ &m_3\ddot{Y}_3 + c\dot{Y}_3 + k_2(Y_3 - Y_2) + k_3(Y_3 - Y_4) = F_{Y_3} - m_3 g \\ &m_4\ddot{X}_4 + c\dot{X}_4 + k_3(X_4 - X_3) = m_4 r\omega^2\cos(\omega t) \\ &m_4\ddot{Y}_4 + c\dot{Y}_4 + k_3(Y_4 - Y_3) = m_4 r\omega^2\sin(\omega t) - m_4 g \end{aligned} \tag{11}$$

where g is the acceleration of gravity, w is the angular velocity of the rotor and F_{X1}, F_{Y1}, F_{X3} and F_{Y3} are the components of the nonlinear forces of the oil film in the plain bearings following OX, OY, r is the eccentricity of the rotor, k_1, k_2, k_3 are the stiffness matrix of the rotor, c is the damping of the system, X_i and Y_i are the horizontal and vertical displacements, m_1 and m_3 are the concentrated masses of the left and right bearings respectively, m_2 and m_4 are the concentrated masses of the compressor and the turbine, respectively. To ease the calculation, the dimensionless transformations are given as follows:

$$\omega t = \tau, e = \frac{r}{C_p}, x_i = \frac{X_i}{C_p}, y_i = \frac{Y_i}{C_p}, \tag{12}$$

with:

$$\frac{d}{dt} = \omega \frac{d}{d\tau}, \frac{d^2}{dt^2} = \omega^2 \frac{d^2}{d\tau^2}, \tag{13}$$

which give:

$$x' = \frac{dx}{d\tau}, y' = \frac{dy}{d\tau}, x'' = \frac{d^2x}{d\tau^2}, y'' = \frac{d^2y}{d\tau^2}. \tag{14}$$

The substitution of the force of the oil film given by Eq. (4) in Eq. (11) written in the following dimensionless form:

$$\begin{aligned}
&x_1'' + \frac{c}{m_1\omega}x_1' + \frac{k_1}{m_1\omega^2}(x_1 - x_2) = \frac{\sigma}{m_1 C_b \omega^2} f_{x1},\\
&y_1'' + \frac{c}{m_1\omega}y_1' + \frac{k_1}{m_1\omega^2}(y_1 - y_2) = \frac{\sigma}{m_1 C_b \omega^2} f_{y1} - \frac{g}{C_b\omega^2},\\
&x_2'' + \frac{c}{m_2\omega}x_2' + \frac{k_1}{m_2\omega^2}(x_2 - x_1) + \frac{k_2}{m_2\omega^2}(x_2 - x_3) = e\cos(\tau),\\
&y_2'' + \frac{c}{m_2\omega}y_2' + \frac{k_1}{m_2\omega^2}(y_2 - y_1) + \frac{k_2}{m_2\omega^2}(y_2 - y_3) = e\sin(\tau) - \frac{g}{C_b\omega^2},\\
&x_3'' + \frac{c}{m_3\omega}x_3' + \frac{k_2}{m_3\omega^2}(x_3 - x_2) + \frac{k_3}{m_3\omega^2}(x_3 - x_4) = \frac{\sigma}{m_3 C_b \omega^2} f_{x3},\\
&y_3'' + \frac{c}{m_3\omega}y_3' + \frac{k_2}{m_3\omega^2}(y_3 - y_2) + \frac{k_3}{m_3\omega^2}(y_3 - y_4)\\
&\qquad = \frac{\sigma}{m_3 C_b \omega^2} f_{y3} - \frac{g}{C_b\omega^2},\\
&x_4'' + \frac{c}{m_4\omega}x_4' + \frac{k_3}{m_4\omega^2}(x_4 - x_3) = e\cos(\tau),\\
&y_4'' + \frac{c}{m_4\omega}y_4' + \frac{k_3}{m_4\omega^2}(y_4 - y_3) = e\sin(\tau) - \frac{g}{C_b\omega^2}.
\end{aligned} \tag{15}$$

To solve the nonlinear equations of the system of Eq. (15), these eight second order equations are decomposed into sixteen first order equations, with the turbine bearing-rotor system model state variables of the MS5002B turbine are introduced as follows:

$$\begin{aligned}
\bar{x} &= \{\bar{x}_1, \bar{x}_2, \bar{x}_3, \bar{x}_4, \bar{x}_5, \bar{x}_6, \bar{x}_7, \bar{x}_8, \bar{x}_9, \bar{x}_{10}, \bar{x}_{11}, \bar{x}_{12}, \bar{x}_{13}, \bar{x}_{14}, \bar{x}_{15}, \bar{x}_{16}\}\\
&= \{x_1, x_1', x_2, x_2', x_3, x_3', x_4, x_4', y_1, y_1', y_2, y_2', y_3, y_3', y_4, y_4'\}.
\end{aligned} \tag{16}$$

Then the equations of motion become:

$$\begin{aligned}
&\bar{x}_1' = \bar{x}_2,\\
&\bar{x}_2' = -\frac{c}{m_1\omega}\bar{x}_2 - \frac{k_1}{m_1\omega^2}(\bar{x}_1 - \bar{x}_3) + \frac{\sigma}{m_1 C_b \omega^2} f_{\bar{x}_1},\\
&\bar{x}_3' = \bar{x}_4,\\
&\bar{x}_4' = -\frac{c}{m_2\omega}\bar{x}_4 - \frac{k_1}{m_2\omega^2}(\bar{x}_3 - \bar{x}_1) - \frac{k_2}{m_2\omega^2}(\bar{x}_3 - \bar{x}_5) + e\cos(\tau),\\
&\bar{x}_5' = \bar{x}_6,\\
&\bar{x}_6' = -\frac{c}{m_3\omega}\bar{x}_6 - \frac{k_2}{m_3\omega^2}(\bar{x}_5 - \bar{x}_3) - \frac{k_3}{m_3\omega^2}(\bar{x}_5 - \bar{x}_7) + \frac{\sigma}{m_3 C_b \omega^2} f_{\bar{x}_5},\\
&\bar{x}_7' = \bar{x}_8,\\
&\bar{x}_8' = -\frac{c}{m_4\omega}\bar{x}_8 - \frac{k_3}{m_4\omega^2}(\bar{x}_7 - \bar{x}_5) + e\cos(\tau),\\
&\bar{x}_9' = \bar{x}_{10},\\
&\bar{x}_{10}' = -\frac{c}{m_1\omega}\bar{x}_{10} - \frac{k_1}{m_1\omega^2}(\bar{x}_9 - \bar{x}_{11}) + \frac{\sigma}{m_1 C_b \omega^2} f_{\bar{x}_9} - \frac{g}{C_b\omega^2},\\
&\bar{x}_{11}' = \bar{x}_{12},\\
&\bar{x}_{12}' = -\frac{c}{m_2\omega}\bar{x}_{12} - \frac{k_1}{m_2\omega^2}(\bar{x}_{11} - \bar{x}_9) - \frac{k_2}{m_2\omega^2}(\bar{x}_{11} - \bar{x}_{13})\\
&\qquad + e\sin(\tau) - \frac{g}{C_b\omega^2},\\
&\bar{x}_{13}' = \bar{x}_{14},\\
&\bar{x}_{14}' = -\frac{c}{m_3\omega}\bar{x}_{14} - \frac{k_2}{m_3\omega^2}(\bar{x}_{13} - \bar{x}_{11}) - \frac{k_3}{m_3\omega^2}(\bar{x}_{13} - \bar{x}_{15})\\
&\qquad + \frac{\sigma}{m_3 C_b \omega^2} f_{\bar{x}_{13}} - \frac{g}{C_b\omega^2},\\
&\bar{x}_{15}' = \bar{x}_{16},\\
&\bar{x}_{16}' = -\frac{c}{m_4\omega}\bar{x}_{16} - \frac{k_3}{m_4\omega^2}(\bar{x}_{15} - \bar{x}_{13}) + e\sin(\tau) - \frac{g}{C_b\omega^2}.
\end{aligned} \tag{17}$$

This representation of the system of equations (17) is of the form $\bar{x}' = f(\bar{x}, \omega)$, with the steady-state equilibrium points $\bar{x}_s$ are represented in the phase space as the solutions of the equilibrium states, i.e., the solutions of the equation $f(\bar{x}_s, \omega) = 0$

For the stability analysis of the MS5002B turbine bearing-rotor system, the stability of the fixed points $\bar{x}_s$ figures out the equilibrium points of the turbine system formally represented by Eq. (17). Hence, the problem that arises is whether the fixed points are stable or not. Suppose that the system of Eq. (17) has a fixed point at $\bar{x} = \bar{x}_s$, the linearization of this system of Eq. (17) around this state of equilibrium, gives:

$$f(\bar{x}) = f(\bar{x}_s) + J_{\bar{x}_s}.(\bar{x} - \bar{x}_s) + O\left((\bar{x} - \bar{x}_s)^2\right), \tag{18}$$

where J is the Jacobian matrix of f evaluated in $\bar{x}_s$, written by:

$$J \equiv \left[J_{ij}\right] \text{ with } J_{ij} \equiv \frac{\partial f_i}{\partial x_j}. \tag{19}$$

Eq. (18) can be transformed into the following form:

$$\frac{d(\bar{x} - \bar{x}_s)}{dt} = J_{\bar{x}_s}.(\bar{x} - \bar{x}_s). \tag{20}$$

Eq. (20) is linear with constant coefficients, its solutions are a sum of exponentials expressed as follows:

$$\overline{x} - \overline{x}_s = \sum_i A_i.\exp(\lambda_i t), \tag{21}$$

where λ_i are the eigenvalues of the problem, knowing that λ_i are solutions of the following system:

$$\det(J - \lambda.I) = 0, \tag{22}$$

where I is the identity matrix and det is the determinant.

The solutions λ_i are real or imaginary, so the stability of the equilibrium state depends on the eigenvalues. We can get two following cases:

- If for every $i \in [1; n]$ thing, $R_e(\lambda_i) \leq 0$ the fixed point $\bar{x}_s$ is stable;
- If it exists $j \in [1; n]$, $R_e(\lambda_i) \succ 0$ the fixed point $\bar{x}_s$ is unstable.

3. Vibrations' bifurcation behavior of MS5002B turbine bearing-rotor system

Modeling of vibrations bifurcation behavior of the MS5002B turbine bearing-rotor system is done in this section, considering the effects of nonlinear forces of the oil film, based on the observed turbine operating state, under de different rotational speed of the rotors. As well as in the presence of instabilities generated by the phenomenon of unbalance on the shaft lines of turbine bearing-rotor system. This nonlinear dynamic will be modeled using the bifurcation diagram, the phase portrait, the Poincaré map and the frequency spectrum, in order to figure out the stable operating zones of the studied turbine and to guarantee a proper operation. Indeed, the theory of bifurcations aims to describe the changes and variations of the points of stability, verifying the equilibrium equations to represent the real behavior of the system. The nonlinear system dynamics is given by:

$$\dot{x} = f(x, \alpha), \tag{23}$$

where $x \in \Re^N$ is the state vector, f is the nonlinear function and α is the control parameter vector.

When the control parameter α is variable, we say that a value α_c is a critical bifurcation value, if the vector field $f(x, \alpha_c)$ is not equivalent to $f(x, \alpha)$ whatever α is in the neighborhood of α_c. However, the bifurcation diagram summarizes all the essential information of the nonlinear dynamic system, which is the case of the studied turbine and helps to understand how its behavior evolves and is a useful means to analyze their stability.

Numerically, we can calculate the bifurcations which connects the equilibriums to the periodic motion is the Hopf bifurcation. The loss of stability at the Hopf bifurcation occurs when a pair of conjugate eigenvalues cross the imaginary axis at the points $\pm w_c$, where the bifurcation parameter reaches the critical value α_c. This implies that the bifurcation condition $Re\,\lambda_{1,2} = 0$ is satisfied and $lm\lambda_{1,2} \neq 0$, this case corresponds to the Hopf bifurcation, also call the Poincaré-Andronov-Hopf bifurcation, this type of bifurcation connects the equilibriums to the periodic oscillation at the well-determined bifurcation point. From where, the study of the bifurcation of Hopf rests on the following assumptions [4,5]:

(1) Suppose that the system of ordinary differential equations $\dot{x} = f(x, \alpha)$ has a fixed point $x = x_s(\alpha)$;

(2) The Jacobian matrix $J_x(x_s(\alpha), \alpha) = \frac{\partial f_i}{\partial x_j}(x_s(\alpha), \alpha)$; $i, j = 1, \ldots, N$ has a pair of complex conjugate eigenvalues $\mu(\alpha) \pm i\beta(\alpha)$, such as when; $\alpha = \alpha_c, \mu(\alpha_c) = 0, \beta(\alpha_c) = \omega_0 > 0$ such that α_c is the critical value of α and the other eigenvalues $(n-2)$ have negative real parts;

(3) The derivative of $\frac{\partial \mu(\alpha)}{\partial \alpha} \neq 0$ when $\alpha = \alpha_c$;

(4) The function f is analytical in x and α in the neighborhood of $(x, \alpha) = (x_s, \alpha_c)$.

If hypothesis (2) holds, then hypothesis (3) implies that the linear stability of the fixed point $x_s(\alpha)$ will be lost when α crosses to α_c. That, allows to describe the model of system by bifurcation of Hopf by the equation of Stuart – Landau, given by:

$$\dot{z} = (\alpha + j\omega_0)z + Lz|z|^2, \omega_0 \neq 0, \mathrm{L} \neq 0. \tag{24}$$

Hence z is the instantaneous complex amplitude and L is the first exponent of the Lyapunov function, if $L \succ 0$, the bifurcation is subcritical and the unstable cycle and the stable focus exist for $\alpha \prec 0$ and only one unstable focus exists for $\alpha \succ 0$ and if $L \prec 0$, the bifurcation is supercritical and the cycle exists and is stable for $\alpha \succ 0$ and the focus is stable for $\alpha \prec 0$ and unstable for $\alpha \succ 0$.

To study this equation (24), the variable z is written in form $z = re^{j\theta}$, where the normal form is written in the polar coordinate system (r, θ) and after the calculations we get:

$$\begin{cases} \dot{r} = \alpha r + Lr^3 \\ \dot{\theta} = \omega_0 \end{cases} \tag{25}$$

where $r = |z|$ and $\theta = \arg(z)$.

Hence, the Hopf bifurcation is the combination of a fork bifurcation $\dot{r}$ and a rotation $\dot{\theta}$ at constant angular speed, from the equation of stationary amplitudes, i.e. $\alpha r + Lr^3 = 0$, we get values of d amplitude for equilibrium $r_f = 0$ and for the limit cycle $r_c^2 = -\alpha/L$. Therefore, the limit cycle exists if $\alpha/L < 0$ and the quantity w_0 gives its period $T = 2\pi/\omega_0$. The eigenvalues result from setting up the determinant D equal to zero, at the equilibriums points determined by:

$$D = \det[J(t) - \lambda I] = (\alpha + 3Lr^2 - \lambda_i)_{r_i} = 0. \tag{26}$$

Therefore, the eigenvalues are obtained as follows:

$$\begin{cases} \lambda_f = \alpha \\ \lambda_c = -2\alpha \end{cases} \tag{27}$$

The numerical results of the developed model show that as the rotational speed increases, the bearing-rotor system undergoes a variety of nonlinear phenomena and complex

dynamic behaviors, including periodic, quasi-periodic and multi-periodic motions. One of the main causes of unstable rotor movement is the effect of the non-linear force of the oil film. The study of their characteristic is therefore a prerequisite for improving the dynamic stability of the system. The obtained results are a useful reference source for the design and control of such a bearing-rotor system of the examined gas turbine.

The application of Hopf's bifurcation theory to the MS5002B turbine bearing-rotor system is based on the study of dynamic behavior given in the equation system of Eq. (17), this formulation having the proper form $\bar{x}' = f(\bar{x}, \omega)$ for the application of Hopf's bifurcation theory. Also, a stationary equilibrium position $\bar{x}_s$ is determined for the rotational speed w, which is considered the control parameter α, when all other system parameters are assumed to be set. So according to Hopf's bifurcation theory, if the parameter w becomes greater than a critical value w_c, implying that there is a stationary point $\bar{x}_s$ will lose its linear stability.

To perform this Hopf bifurcation analysis, firstly, the function f of the system of Eq. (17) is used with a Taylor series around the equilibrium point $\bar{x}_s$, as follows:

$$f(\bar{x},\omega) = f(\bar{x}_s,\omega) + \frac{\partial f}{\partial \bar{x}}(\bar{x}_s,\omega)(\bar{x}-\bar{x}_s) + \frac{1}{2!}\frac{\partial^2 f}{\partial \bar{x}^2}(\bar{x}_s,\omega)(\bar{x}-\bar{x}_s)^2 + \frac{1}{3!}\frac{\partial^3 f}{\partial \bar{x}^3}(\bar{x}_s,\omega)(\bar{x}-\bar{x}_s)^3 + ... \quad (28)$$

Hence the term $f(\bar{x}_s, \omega) = 0$ is used to determine the equilibrium point, the term $\frac{\partial f}{\partial \bar{x}}(\bar{x}_s, \omega)$ used to determine dynamic performance through eigenvalue analysis, the terms $\frac{\partial^2 f}{\partial \bar{x}^2}(\bar{x}_s, \omega)$ and $\frac{\partial^3 f}{\partial \bar{x}^3}(\bar{x}_s, \omega)$ are used to determine the stability of periodic solutions.

In this sense, the nonlinear dynamic behavior of the MS5002B gas turbine bearing-rotor system at high pressure is decided using this proposed analytical model, to obtain the nonlinear dynamic response of displacement and speed of rotations of the studied turbine bearing-rotor system, with calculations and numerical integrations using the bifurcation diagram, phase portrait, Poincaré map and frequency spectrum. This transforms the resolution of the nonlinear problem into that of a succession of a linear system, which is highlighted in the following section of results of investigations and application.

4. Investigations and analysis of the obtained results

In this section, we present the investigations and analysis of the obtained results to highlight the experimental application of bifurcation studies to the examined MS5002B gas turbine. First, we model the turbine bearing-rotor system parameters and initialize them to characterize the nonlinear dynamics of this system. We model the operating zones in periodic and quasi-periodic regimes to mitigate instability effects. Then, we present the different dynamic behaviors of the turbine bearing-rotor system using bifurcation diagram formalisms, phase portrait, Poincaré map, and frequency spectrum. We present the most meaningful results to show the solution of bifurcation problems adapted for the examined gas turbine MS5002B.

Figure 5. Position of the vibration sensor.

For this work, we use data acquisition equipment of Bently Nevada BN3500 type. It consists of a vibration sensor at bearing No. 1, a magnetic sensor (Magnetic Speed Pickup) to measure the speed of rotation, and a thermocouple sensor to measure the temperature variation of the oil film in bearing No. 1. The positions of various sensors are shown in Figures 5 and 6.

4.1. Parameters' modeling of the examined bearing-rotor system

In this section of work, the modeling parameters of the examined MS5002B turbine bearing-rotor system are determined, to characterize the nonlinear dynamics of this system using three bifurcation analysis techniques using frequency spectra, the phase portraits and the Poincaré maps. These three bifurcation diagrams are chosen to study the nonlinear dynamic behaviors of the studied turbine bearing-rotor system, with is a system representation made from the various input/output turbine operating data MS5002B. However, the choice of variables describing the behavior of the bearing-rotor system and the phenomena of instability of this system are considered, as a function of their vibratory influence on this rotating machine. Hence, series of turbine operating data corresponding to the different rotational speed variations of the bearing-rotor system is used to analyze the different behaviors affecting the turbine operating areas. Where, 400 cycles of turbine bearing-rotor response data are used, with 139 first cycles of transient bearing-rotor response excluded to eliminate turbine starting impacts and 261 cycles of bearing-rotor response for rpm permanent are exploited, to reproduce the vibratory behaviors of the turbine, making it possible to determine the optimal speed with the purpose to operate the turbine in the established stable zone. For this, the initial values adopted for the gas turbine bearing-rotor system model MS5002B are given by Table 4, with a numerical integration step equal to $\pi/36$.

In this section, we present the investigations and analysis of the obtained results to highlight the experimental application of bifurcation studies to the MS5002B gas turbine. First, we model the turbine bearing-rotor system parameters and initialize them to characterize the nonlinear dynamics of this system. We model the operating zones in periodic and quasi-periodic regimes to reduce instability

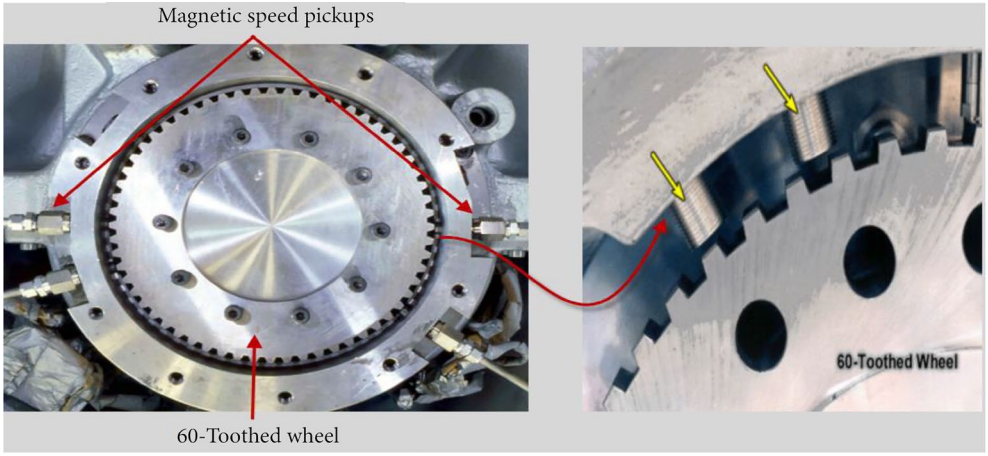

(a)

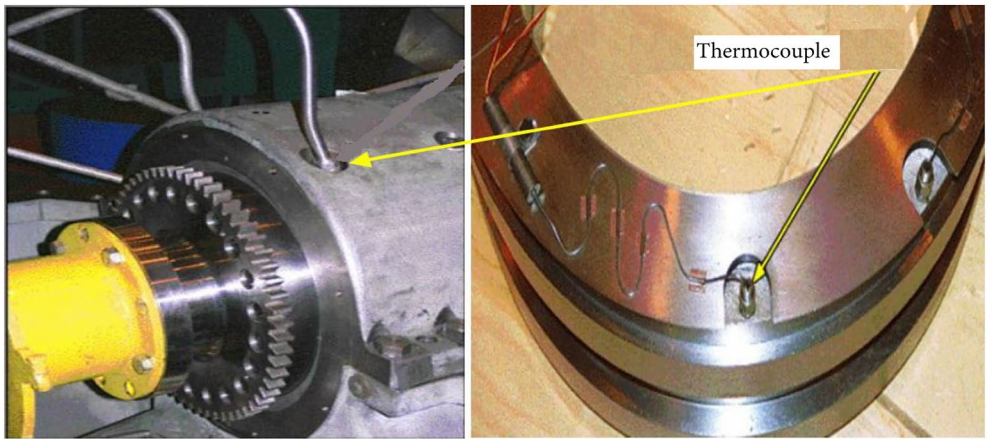

(b)

Figure 6.A: Position of the magnetic pickup (Magnetic speed pickup); (b) Position of the thermocouple sensor.

Table 4. Parameters of the studied turbine bearing-rotor system.

Parameters	Values	Units
Concentrated mass of left-hand bearings N°1 m_1	50	[kg]
Concentrated mass of the compressor m_2	6480	
Concentrated mass of right-hand bearings N°2 m_3	50	
Concentrated mass of turbine m_4	200	
Rotor stiffness k	8×10^6	[N/m]
Rotor damping c	500	[N.s/m]
Ray R	101.89	[mm]
Length L	122.27	
Radial clearance of the bearing C_b	0.2	
Rotor eccentricity r	0.06	[mm]
Dynamic viscosity μ	0.03	[Pa.s]

effects. Then, we present the different dynamic behaviors of the turbine bearing-rotor system using three bifurcation analysis techniques: frequency spectra, phase portraits, and Poincaré maps. We base the system representation on various input/output turbine operating data from the MS5002B.

The choice of variables to describe the behavior of the bearing-rotor system and the instability phenomena is made considering their vibratory influence on the rotating machine. We employ a series of turbine operating data corresponding to variations in the rotational speed of the bearing-rotor system to analyze the different behaviors affecting the turbine within its operational zones. Specifically, we use 400 cycles of turbine bearing-rotor response data. The first 139 cycles of transient bearing-rotor response are excluded to eliminate the impacts of turbine starting, leaving us with 261 cycles of bearing-rotor response for maintaining a constant RPM. This data enables us to replicate the vibratory behaviors of the turbine and determine the optimal speed for operating the turbine within the established stable zone.

The initial values adopted for the gas turbine bearing-rotor system model MS5002B are outlined in Table 4, with a numerical integration step equal to $\pi/36$, are given by:

$$\bar{x}_{0i} = \{\bar{x}_{01}, \bar{x}_{02}, \cdots, \bar{x}_{016}\} = \left\{\begin{matrix} 10^{-5}, 10^{-4}, 10^{-5}, 25.7\times10^{-3}, 10^{-5}, -35.8\times10^{-4}, 0^{-5}, 36.4\times10^{-5}, \\ 10^{-5}, 8\times10^{-5}, 10^{-5}, 47\times10^{-8}, 10^{-5}, 52\times10^{-5}, 10^{-5}, -32.14\times10^{-5} \end{matrix}\right\}$$

Practically, the bifurcation diagram is a graphical representation where the x-axis signifies the bifurcation parameter undergoing alteration (in our case, the angular velocity ω), and the y-axis depicts the observed system behavior.

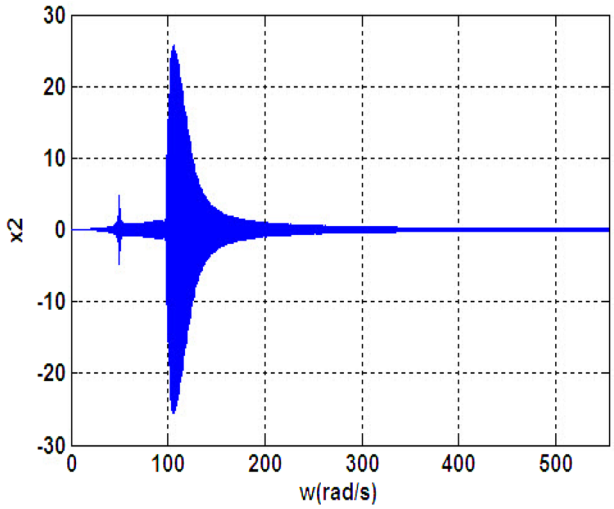

Figure 7: Bifurcation diagram of the compressor center.

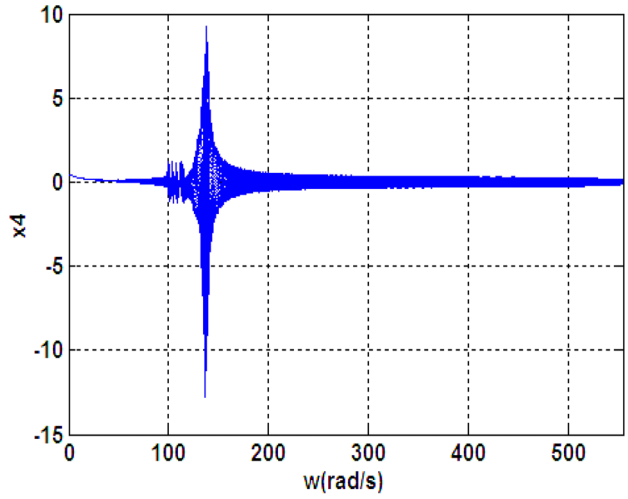

Figure 8. Bifurcation diagram of the turbine center.

Different types of behavior, such as stable points, periodic orbits, and chaotic behavior, will later be presented in this section through distinctive patterns or structures in the diagram.

The variations in the different bifurcation diagrams, presented in Figures 7 and 8 are plotted as a function of the angular speed of rotation of the turbine rotor. These diagrams reveal the areas of instability linked to various turbine operating speed models.

4.2. Dynamic behavior of the examined turbine bearing-rotor system

To investigate the dynamic behaviors of the bearing-rotor system within various ranges of angular speed variations, a data acquisition system has been established on the examined turbine. This system comprises different sensors strategically positioned on the bearing-rotor system to observe the movements of the system as it operates during turbine operation.

However, Figure 9 shows the periodic motion of the turbine center at $\omega = 98$ rad/s with double period time $2T_0$, waveform in the horizontal direction of x_4, as shown in Figure 9(a), for this periodic motion. Hence, in the frequency spectrum of Figure 9(b), there are two discrete frequency components corresponding to the rotational speed $\frac{1}{2}f_r$ and f_r is a limited circle in the phase portrait of Figure 9(c), where the trajectory of center of the turbine is regular given by the two discrete points in the Poincaré map of Figure 9(d), which implies that this movement is stable with double period $T = 2 \times T_0 = 4\pi$.

With the increase of the turbine angular speed in the interval $98 < \omega < 200$ rad/s, there is an appearance of the quasi-periodic motion in the center of the turbine and in the center of the rotor in bearing N°2 as shown in Figure 10 at the angular speed of $\omega = 110$ rad/s. Hence, Figure 10 shows the quasi-periodic motion of the center of the time waveform turbine in the direction x_4 as shown in Figure 10(a) at the critical speed $\omega = 110$ rad/s, there are two components discrete frequencies with vibration amplitudes in the order of 0.33 and 0.39 as shown in Figure 10(b), corresponding to the speed of rotation f_r and $\frac{9}{4} \times f_r$, with a risk of increased amplitude of turbine rotor vibrations. As well as several vibration modes can appear during turbine operation because the trajectories are very disordered in the limit circles in the phase portrait of Figure 10(c). Moreover, the projections of the Poincaré section of Figure 10(d) are of the closed curve type, indicating the quasi-periodic nature of the movement of the turbine bearing-rotor system, which can be interpreted by the strong presence of the force effects of the non-linear oil film.

And when the turbine angular speed varied in the interval $200 \leq \omega \leq 555$ rad/s, the dynamic motion of bearing-rotor system changes from a quasi-periodic motion to a periodic motion. In this range of rotation, the results obtained from periodic movement from turbine center at $\omega = 300$ rad/s with NT_0 periods as given in Figure 11 of a time waveform x_4 shown in Figure 11(a), shows that there are two dynamics discrete frequency vibrators corresponding to the speed of rotation $\frac{4}{9} \times f_r$ and f_r with the frequencies 0.27 and 0.06 is a negligible dynamic with a frequency on the order of 0.01, as shown in Figure 11(b). This causes the existence of a limited circle in the phase portrait presented in Figure 11(c), where the trajectory is regular, with the presence N of discrete points in the Poincaré maps of Figure 11(d), which proves that the movement is periodic with a period of $T = N \times T_0 = N \times 2\pi$.

To recognize the dynamic behavior of compressor center over an interval of angular speed $1 \leq \omega \leq 555$ rad/s, Figure 12 shows the evolution of their periodic motion at $\omega = 10$ rad/s with four periods $4T_0$, where Figure 12(a) shows the waveform temporal movement of x_2, Figure 12(b) shows the variation in frequency spectrum of this movement, Figure 12(c) shows the phase portrait of y_2 as function of x_2 and Figure 12(d) shows their projections according to the Poincaré map. However, a bifurcation diagram was obtained on the interval $1 \leq \omega \leq 22$ rad/s, where the movement is periodic for four periods $T = 4 \times T_0 = 8\pi$, in the case of $\omega = 10$ rad/s a limit cycle appears as the critical value of stability, in the phase portrait with trajectory regular and four discrete points in the Poincaré map, for these turbine rotor rotation amplitude values.

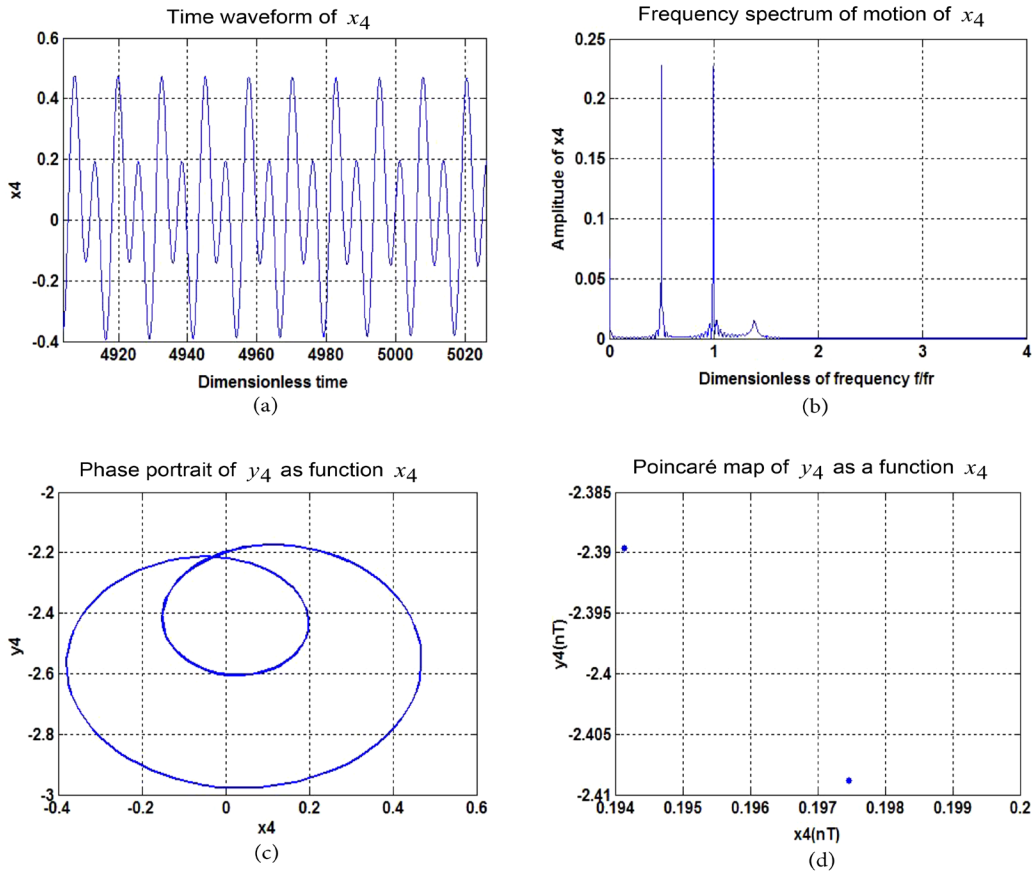

Figure 9. Periodic motion of the turbine center at $w = 98$ rad/s with double period $2T_0$, (a) Time waveform of x_4, (b) Frequency spectrum of motion of x_4, (c) Phase portrait of y_4 as function x_4, and (d) Poincaré map of y_4 as a function x_4.

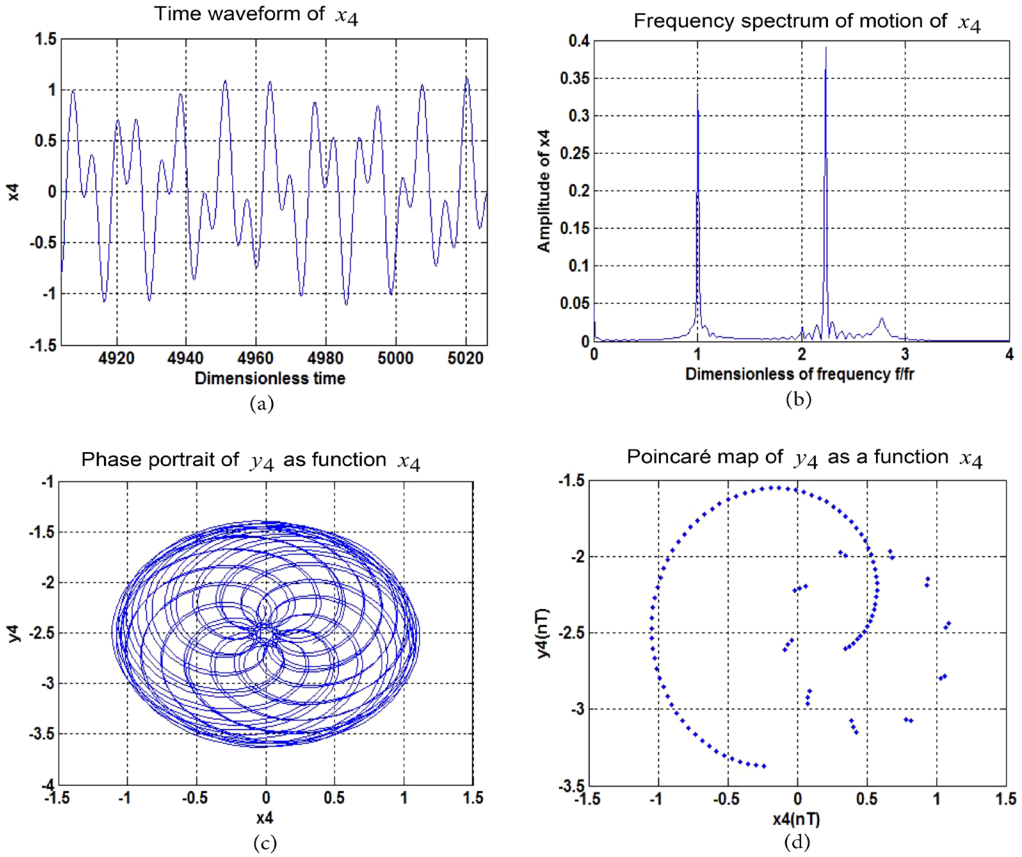

Figure 10. Quasi-periodic movement of turbine center at $w = 110$ rad/s, (a) Time waveform of x_4, (b) Frequency spectrum of motion of x_4, (c) Phase portrait of y_4 as function x_4, and (d) Poincaré map of y_4 as a function x_4.

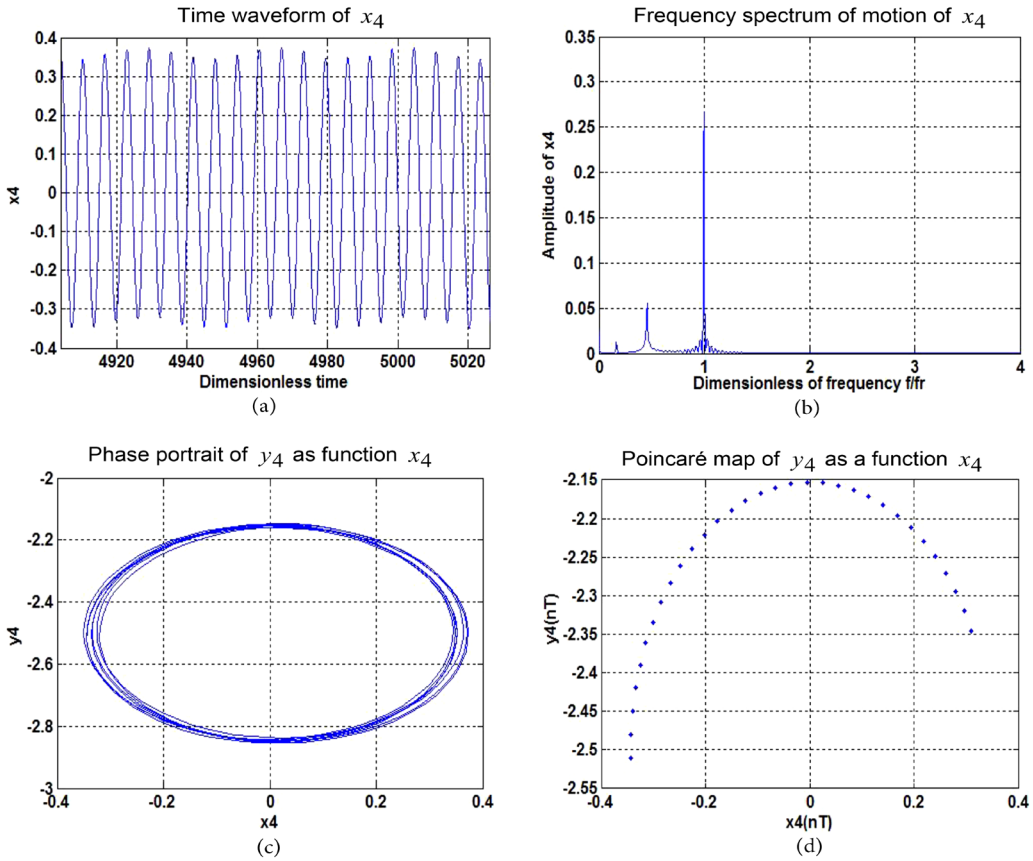

Figure 11. Periodic movement of turbine center at $w = 300$ rad/s with NT_0 periods, (a) Time waveform of x_4, (b) Frequency spectrum of motion of x_4, (c) Phase portrait of y_4 as function x_4, and (d) Poincaré map of y_4 as a function x_4.

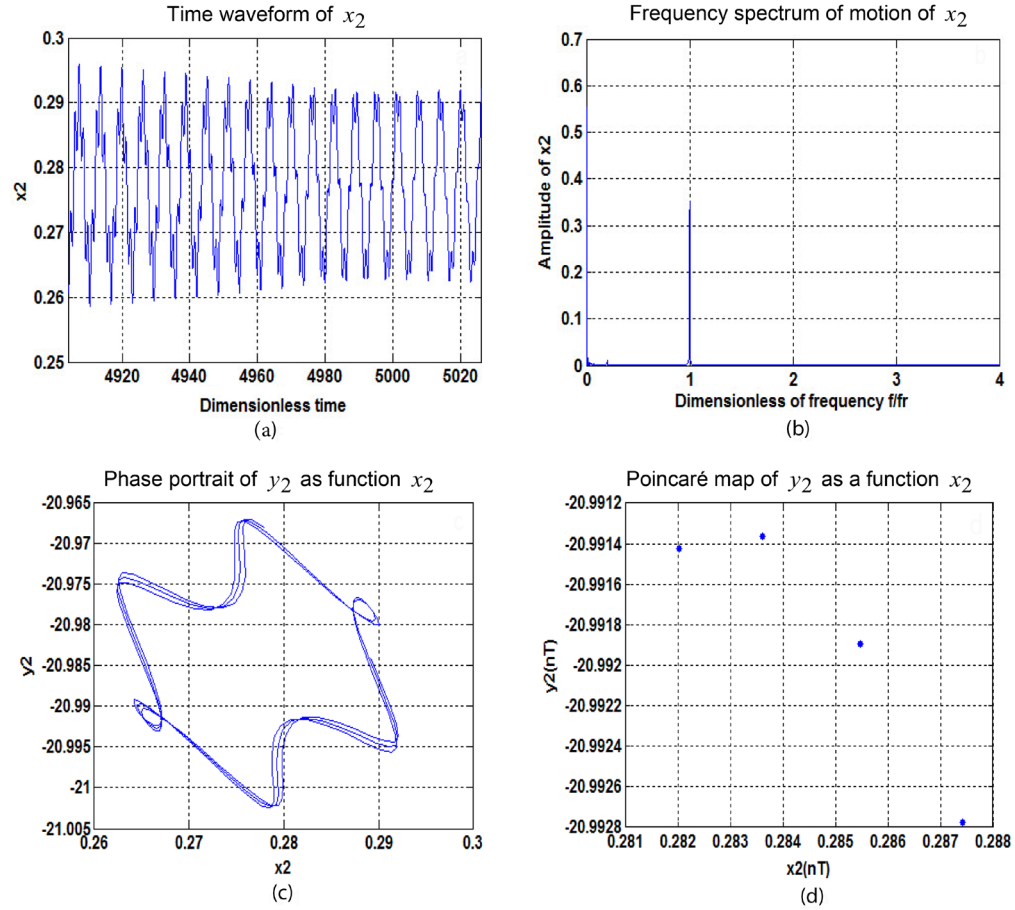

Figure 12. Periodic movement of compressor center at $w = 10$ rad/s with four periods $4T_0$, (a) Time waveform of x_2, (b) Frequency spectrum of motion of x_2, (c) Phase portrait of y_2 as function x_2, and (d) Poincaré map of y_2 as a function x_2.

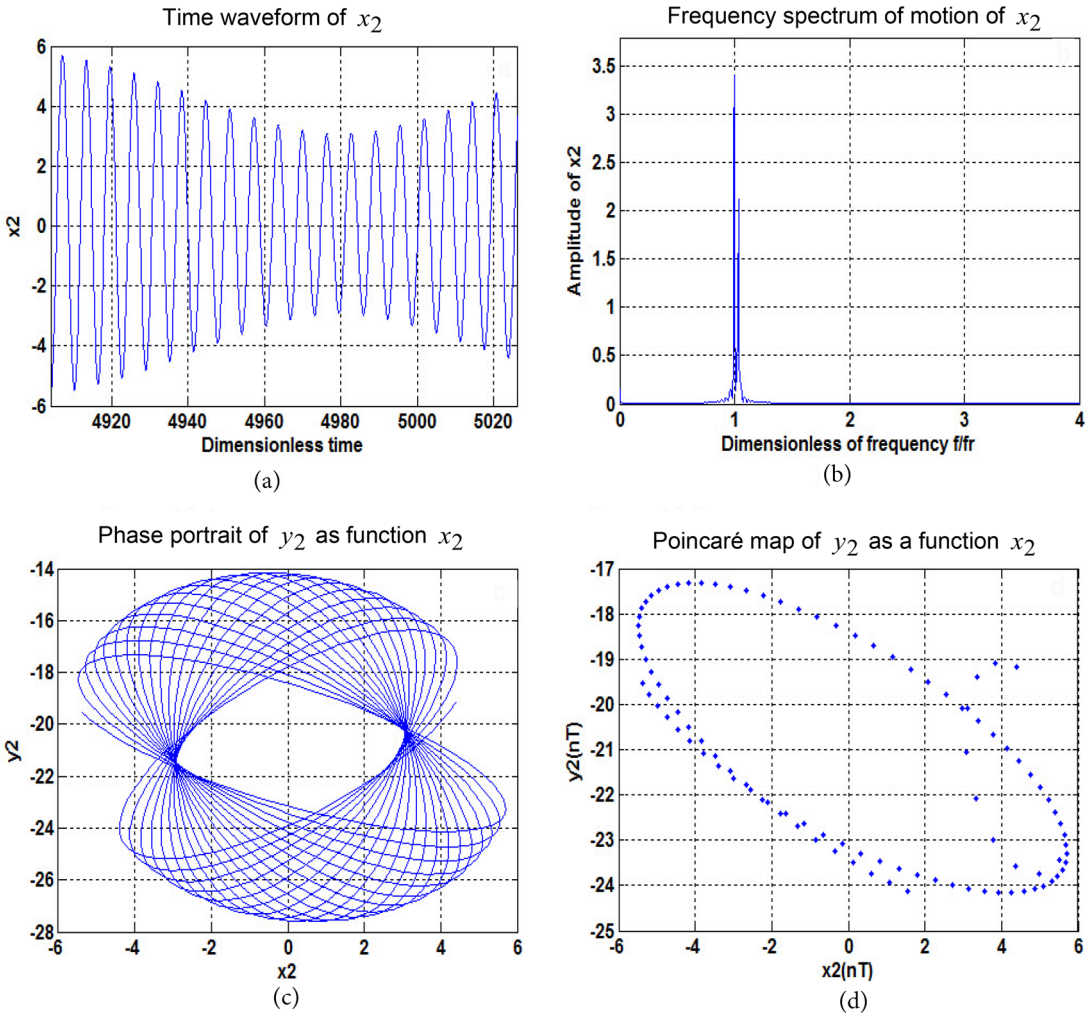

Figure 13. Quasi-periodic movement of compressor center at $w = 110$ rad/s, (a) Time waveform of x_2, (b) Frequency spectrum of motion of x_2, (c) Phase portrait of y_2 as function x_2, and (d) Poincaré map of y_2 as a function x_2.

The results obtained in Figure 13 show the quasi-periodic movement of the compressor center at the critical speed $\omega = 110$ rad/s with temporal integration of this quasi-periodic movement and which indicates the presence of partial contacts with the turbine rotor due to the effects of unbalance and the force effects of the oil film. This implies the rapid increase in the amplitudes of vibrations, as shown in Figure 13(b) of the time-wave motion frequency spectrum of x_2 as given in Figure 13(a), which can reach up to the amplitude of 3.4. Hence, the phase portrait trajectories of y_2 as a function of x_2 given in Figure 13(c) are disordered with projections on the map of the Poincaré section of Figure 13(d) of closed curve type. These results appear to be an advance for practical measurements of these type of gas turbine vibration modes.

For speed variations in $200 \leq \omega \leq 555$ rad/s, the periodic motion from compressor center at $\omega = 300$ with N periods NT_0 is shown in Figure 14, with the data time wave motion x_2 given in Figure 14(a) and the frequency spectrum of this movement given in Figure 14(b), after this speed the movement of the rotor is no longer quasi-periodic and passes to a periodic movement. In addition, this return to this periodic regime is established by determining a stable limit cycle at the value of this critical speed, what is shown on the phase portrait of y_2 as a function of x_2 given in Figure 14(c) and projected on their Poincaré map in the Figure 14(d).

The actual operating data of the examined gas turbine MS5002B in this work is designed to measure the dynamic characteristics of the bearing-rotor system under a series of conditions, such as a full set of different operating processes. Hence, the numerical results of the modeling made are validated by the experimental data, to monitor the dynamic behavior of the bearing-rotor system. Figure 15 shows the variation of movement of the center of the rotor in the bearings N° 1 in parallel with the variation of the angular speed of the rotor HP and the temperature of the film of oil, these variations break down into two phases, phase of starting and maximum operating phase. Where, the vibrations evolve according to the angular velocity and the temperature of the oil film. Knowing that, the variation of the film temperature greatly affects the viscosity of the oil and on the other hand the strength of the oil film is highly dependent on the viscosity of the oil such as a decrease in pressure or an increase oil film temperature causes a decrease in oil film viscosity and strength.

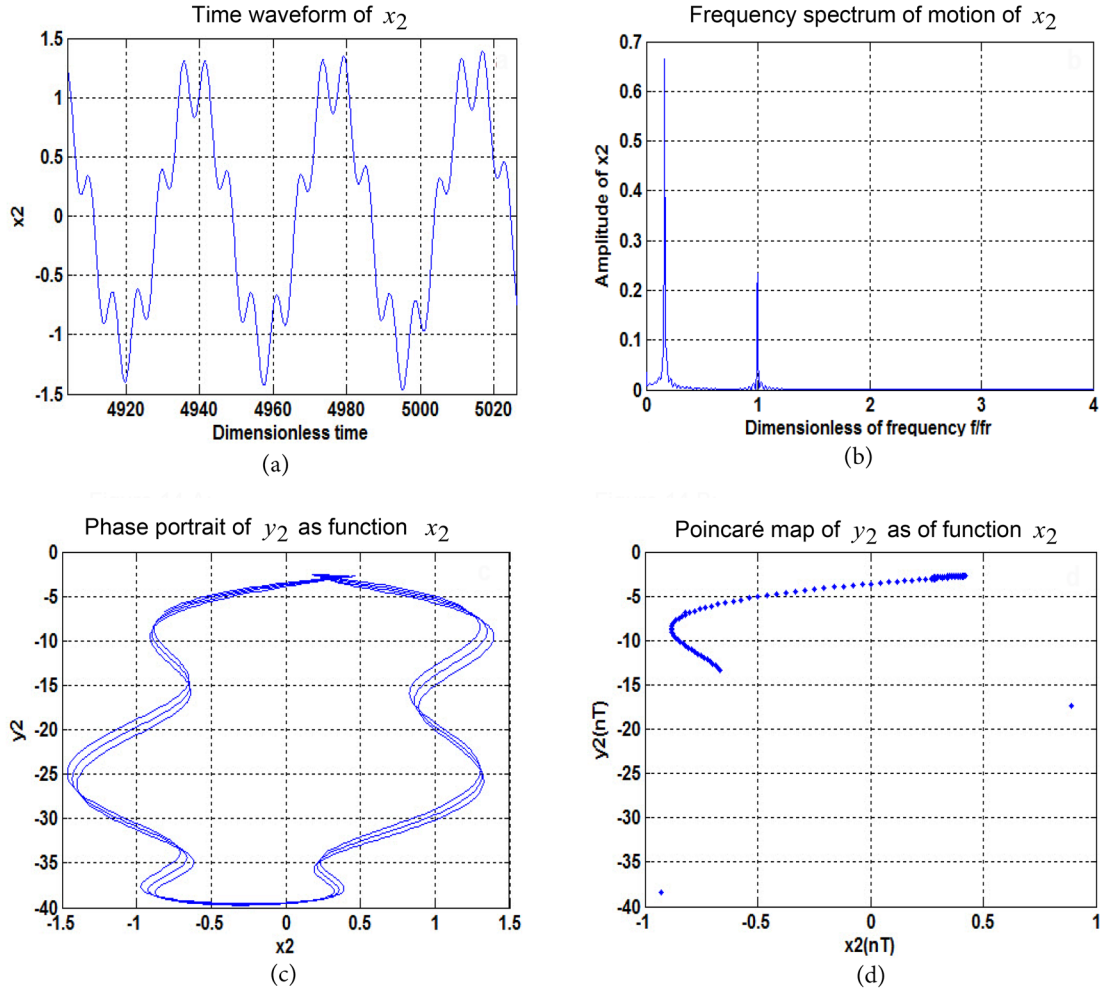

Figure 14. Periodic movement of compressor center at $w = 300$ rad/s with NT_0 periods, (a) Time waveform of x_2, (b) Frequency spectrum of motion of x_2, (c) Phase portrait of y_2 as function x_2, and (d) Poincaré map of y_2 as of function x_2.

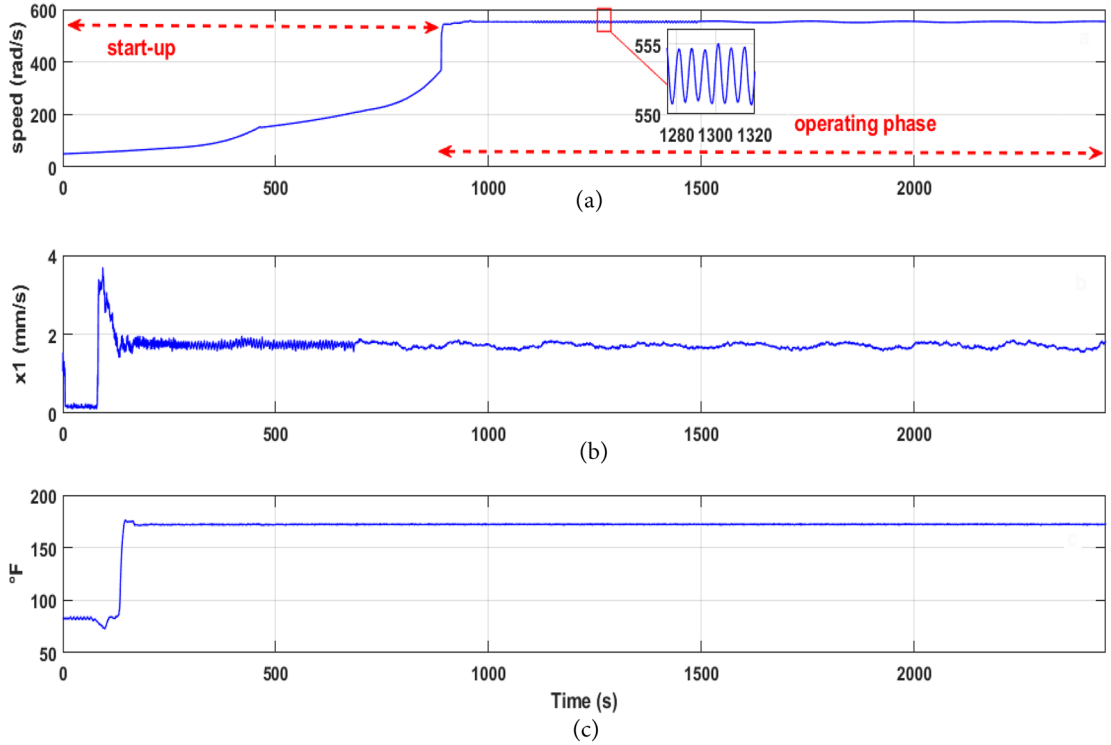

Figure 15. Dynamic behavior of the bearing-rotor system in bearing N°1 (a) rotor speed HP, (b) movement of the center of the rotor, (c) temperature of the oil film.

Also, it is clear that when the angular velocity is low such as ω ≤55 rad/s and t ≤70 s, only low amplitude synchronous vibrations appear. This synchronous movement is caused by the inertial force of the unbalance of the HP rotor. When the angular velocity increases further so that 55 rad/s < ω < 210 rad/s and 70 s < t < 695 s, an oil whirl appears, which results in an increase in amplitude of vibrations and a decrease in the temperature of the oil film in 55 rad/s <ω ≤57 rad/s and 77 s < t ≤97 s following a decrease in the amplitude of vibrations and increase in the temperature of the oil film in 57 rad/s <ω <210 rad/s and 97 s < t <695 s. So, in this range of 55 rad/s <ω <210 rad/s the system will vibrate strongly and become unstable, oil swirl usually occurs when there is a change in oil properties such as temperature and oil viscosity. It is a mechanism for converting rotational energy into vibrational energy through the force of the oil film.

As the angular velocity increases so that 210 rad/s ≤ ω ≤ 555 rad/s and 695 s ≤ t ≤ 2445 s i.e., until the maximum operating phase, the vortex of oil disappears. At this range, the quenching phenomenon occurs because the increasing synchronous vibrations suppress the oil swirl, and the system becomes more stable. As well as the vibration amplitude caused by oil swirl is greater than that of synchronous vibration. So, based on the obtained experimental results through this study, we can conclude that there is an agreement between the experimental results and the numerical results of the developed model with a relative deviation of ≈ 1%.

5. Conclusion

This research has emphasized the experimental exploration of vibration bifurcation diagrams for the MS5002B turbine bearing-rotor system. The study has introduced reliable models characterizing the vibration bifurcation behaviors affecting the examined turbine, thereby shedding light on the areas of stable operation. The investigation considered undesirable effects contributing to the instability of the bearing-rotor system, such as imbalance, non-linear film forces, rotor contacts, rotor misalignment, and other sources of vibration.

Within this context, the study applied bifurcation diagram analysis to understand vibratory phenomena and monitor the operational state of the MS5002B. This involved an examination of the nonlinear dynamics exhibited by the bearing-rotor system. Concepts related to bifurcation theory, including phase portraits, various Poincaré maps, and frequency spectra, were employed to gain better insights into the destabilizing effects impacting the examined turbine. This allowed the utilization of digital advancements to effectively employ advanced tools for analyzing complex instability phenomena and ensuring the stable and safe operation of the turbine.

The results obtained from various tests on the bearing-rotor system of the MS5002B turbine demonstrated the robustness of the bifurcation models developed for variable turbine speeds. Furthermore, this work underscored the potential and performance of bifurcation tracking algorithms in the analysis of complex dynamic behaviors in gas turbines. These algorithms have proven effective in detecting harmonic resonances in the spectra of vibratory frequencies, serving as a valuable tool for developing systems that support the monitoring and diagnosis of gas turbines. This, in turn, ensures equipment sustainability by averting unexpected failures. The use of vibration analysis in conjunction with bifurcation indicators aids in the detection of limit points with periodic, quasi-periodic, or multi-periodic solutions, making it possible to identify vibration faults and track their changes over time, thus preventing the degradation of the studied turbine.

Nomenclature

Q_1	Rotor center in bearing N° 1
Q_2	Compressor center
Q_3	Rotor center in bearing N° 2
Q_4	Turbine center
k_1, k_2 and k_3	Shaft stiffness matrix of the rotor
R	Radius of bearing
L	Length of bearing
z	Dimensionless axial displacement
p	Dimensionless pressure of the oil film
C_b	Radial clearance of the bearing
	x and y dimensionless horizontal and vertical displacements
h	Dimensionless thickness of the oil film
e	Relative eccentricity of rotor
X_i, Y_i	Horizontal and vertical displacements
τ	Dimensionless time
f_r	Rotational frequency
σ	Sommerfeld number
μ	Dynamic viscosity
f_x and f_y	Dimensionless nonlinear forces of the oil film
g	Acceleration of gravity
w	Angular velocity of the rotor
F_{X1}, F_{Y1}, F_{X3} and F_{Y3}	Components of the nonlinear forces of the oil film
r	Eccentricity of the rotor
c	Damping of the system
X_i, Y_i	Horizontal and vertical displacements
m_1	Concentrated masses of the of bearing N°1
m_3	Concentrated masses of the of bearing N°2
m_2	Concentrated masses of the compressor
m_4	Concentrated masses of the turbine
$\bar{x}_s$	Equilibrium points
J	Jacobian matrix
λ_i	Eigenvalues
I	Identity matrix
f	Nonlinear function
α	Control parameter vector
α_c	Critical bifurcation value
D	Determinant
w_c	Critical value of rotation
μ	Dynamic viscosity
r	Rotor eccentricity
c	Rotor damping
k	Rotor stiffness

Acknowledgments

The authors express their sincere gratitude to the General Directorate of Scientific Research and Technological Development (DGRSDT), Algeria, for their support during the execution of this

work at the Applied Automation and Industrial Diagnostics Laboratory, University of Djelfa, Algeria.

Funding

This research did not receive any specific grant from funding agencies in the public, commercial, or not-for-profit sectors.

Conflicts of interest

The authors declare that they have no known competing financial interests or personal relationships that could have appeared to influence the work reported in this paper.

Authors contribution statement

Frist author
Youcef Mahroug: Conceptualization, Methodology, Investigation; Writing – original draft.

Second author

Ahmed Hafaifa: Supervision; Formal Analysis; Validation; Writing –review and editing.

Third author

Abdelhamid Iratni: Data Curation; Software, Validation; Writing – review and editing.

Fourth author

Mouloud Guemana: Resources; Investigation; Project administration; Writing –review and editing.

Fifth author

Ilhami Colak: Supervision; Visualization; Project administration; Writing – review and editing.

References

1. Wang, J.K. and Khonsari, M.M. "Bifurcation analysis of a flexible rotor supported by two fluid-film journal bearings", *Journal of Tribology*, **128**, pp. 594-603 (2006). https://doi.org/10.1115/1.2197842

2. Wang, J.K. and Khonsari, M.M. "Influence of inlet oil temperature on the instability threshold of rotor-bearing systems", *Journal of Tribology*, **128**, pp. 319-326 (2006). https://doi.org/10.1115/1.2162920

3. Chasalevris, A., Dohnal, F., and Chatzisavvas, I. "Experimental detection of additional harmonics due to wear in journal bearings using excitation from a magnetic bearing", *Tribology International*, **71**, pp. 158-167 (2014). https://doi.org/10.1016/j.triboint.2013.12.002

4. Miraskari, M., Hemmati, F., and Gadala, M.S. "Nonlinear dynamics of flexible rotors supported on journal bearings—Part I: Analytical bearing model", *Journal of Tribology*, **140**(2), 021704 (2018). https://doi.org/10.1115/1.4037730

5. Miraskari, M., Hemmati, F., and Gadala, M.S. "Nonlinear dynamics of flexible rotors supported on journal bearings—part II: numerical bearing model", *Journal of Tribology*, **140**(2), 021705 (2018). https://doi.org/10.1115/1.4037731

6. Anastasopoulos, L. and Chasalevris, A. "Bifurcations of limit cycles in rotating shafts mounted on partial arc and lemon bore journal bearings in elastic pedestals", *Journal of Computational and Nonlinear Dynamics*, **17**(6), p. 061003 (2022). https://doi.org/10.1115/1.4053593

7. Noah, S.T. and Sundararajan, P. "Significance of considering nonlinear effects in predicting the dynamic behavior of rotating machinery", *Journal of Vibration and Control*, **1**(4), pp. 431-458 (1995). https://doi.org/10.1177/107754639500100403

8. Mahroug, Y., Khaldi, B.S., Guemana, M., et al. "ARMAX-based identification and diagnosis of vibration behavior of gas turbine bearings", *Diagnostyka*, **24**(3). 2023310 (2023). https://doi.org/10.29354/diag/171277

9. Ehrich, F. "Observations of subcritical superharmonic and chaotic response in rotordynamics", *Journal of Vibration and Acoustics*, **114**(1), pp. 93-100 (1992). https://doi.org/10.1115/1.2930240

10. Wu, B. "Dynamic performance simulation analysis method of split shaft gas turbine based on RBF neural network", *Energy Reports*, **7**, pp. 947-958 (2021). https://doi.org/10.1016/j.egyr.2021.09.178

11. Ju, J., Li, W., Wang, Y., et al. "Dynamics and nonlinear feedback control for torsional vibration bifurcation in main transmission system of scraper conveyor direct-driven by high-power PMSM", *Nonlinear Dynamics*, **93**, pp. 307-321 (2018). http://dx.doi.org/10.1007/s11071-018-4193-2

12. Li, Z., Li, J., and Li, M. "Nonlinear dynamics of unsymmetrical rotor-bearing system with fault of parallel misalignment", *Advances in Mechanical Engineering*, **10**(5), pp.1-17 (2018). https://doi.org/10.1177/1687814018772908

13. Hafaifa, A., Guemana, M., and Daoudi, A. "Vibrations supervision in gas turbine based on parity space approach to increasing efficiency", *Journal of Vibration and Control*, **21**(8), pp. 1622-1632 (2015). https://doi.org/10.1177/1077546313499927

14. Djeddi, C., Hafaifa, A., Iratni, A., et al. "Robust diagnosis with high protection to gas turbine failures identification based on a fuzzy neuro inference monitoring approach", *Journal of Manufacturing Systems*, **59**, pp. 190-213 (2021). https://doi.org/10.1016/j.jmsy.2021.02.012

15. Mohamadi, A., Shahgholi, M., and Ashenai Ghasemi, F. "Nonlinear dynamic and bifurcations analysis of an axially moving circular cylindrical nanocomposite shell", *International Journal of Mechanics and Materials in Design*, **18**(1), pp. 125-154 (2022). https://doi.org/10.1007/s10999-021-09571-9

16. Avramov, K. and Malyshev, S. "Bifurcations and chaotic forced vibrations of cantilever beams with breathing cracks", *Engineering Fracture Mechanics*, **214**, pp. 289-303 (2019). https://doi.org/10.1016/j.engfracmech.2019.03.021

17. Avramov, K. and Raimberdiyev, T. "Bifurcations behavior of bending vibrations of beams with two breathing cracks", *Engineering Fracture Mechanics*, **178**, pp. 22-38 (2017). https://doi.org/10.1016/j.engfracmech.2017.04.006

18. Aghayari, J., Bab, S., Safarpour, P., et al. "A novel modal vibration reduction of a disk-blades of a turbine using nonlinear energy sinks on the disk", *Mechanism and Machine Theory*, **155**, 104048 (2021). https://doi.org/10.1016/j.mechmachtheory.2020.104048

19. Ma, L., Yao, M., Zhang, W., et al. "Bifurcation and dynamic behavior analysis of a rotating cantilever plate in subsonic airflow", *Applied Mathematics and Mechanics*, **41**, pp. 1861-1880 (2020). https://doi.org/10.1007/s10483-020-2668-8

20. Noiray, N. and Schuermans, B. "Deterministic quantities characterizing noise driven Hopf bifurcations in gas turbine combustors", *International Journal of Non-Linear Mechanics*, **50**, pp. 152-163 (2013). https://doi.org/10.1016/j.ijnonlinmec.2012.11.008

21. Mao, X.Y., Gao, S.Y., Ding, H., et al. "Static bifurcation and nonlinear vibration of pipes conveying fluid in thermal environment", *Ocean Engineering*, **278**, 114418 (2023). https://doi.org/10.1016/j.oceaneng.2023.114418

22. Chasalevris, A. "Stability and Hopf bifurcations in rotor-bearing-foundation systems of turbines and generators", *Tribology International*, **145**, p. 106154 (2020). https://doi.org/10.1016/j.triboint.2019.106154

23. Wang, X., Long, X., Yue, X., et al. "Bifurcation analysis of stick–slip vibration in a 2-DOF nonlinear dynamical system with dry friction", *Communications in Nonlinear Science and Numerical Simulation*, **111**, p. 106475 (2022). https://doi.org/10.1016/j.cnsns.2022.106475

24. Zheng, Y., Wang, G., Zhu, Q., et al. "Bifurcations and nonlinear dynamics of asymmetric tri-stable piezoelectric vibration energy harvesters", *Communications in Nonlinear Science and Numerical Simulation*, **119**, 107077 (2023). https://doi.org/10.1016/j.cnsns.2022.107077

25. Asghari, H. and Dardel, M. "Parameter converting method for bifurcation analysis of nonlinear dynamical systems", *Scientia Iranica*, **27**(1), pp. 310-329 (2020). https://doi.org/10.24200/sci.2018.50714.1832

26. Baum, C., Leister, T., and Seemann, W. "Stability and bifurcation analysis of a rotor in rigid and foil air bearings utilized for the identification of the air whirl effect", *Journal of Sound and Vibration*, **536**, 117067 (2022). https://doi.org/10.1016/j.jsv.2022.117067

27. Zhuang, G., Zong, W., and Tang, Y. "Statistical analysis and suppression of vibration frequency bifurcation in diamond turning of Al 6061 mirror", *Mechanical Systems and Signal Processing*, **198**, p. 110421 (2023). https://doi.org/10.1016/j.ymssp.2023.110421

28. Jahangiri, M. and Bagheri, E. "Effect of radially functionally graded materials on the primary resonances of large amplitude flexural vibration of in-extensional rotating shafts", *Engineering Structures*, **226**, p. 111362 (2021). https://doi.org/10.1016/j.engstruct.2020.111362

29. Li, Y.G. "Aero gas turbine flight performance estimation using engine gas path measurements", *Journal of Propulsion and Power*, **31**(3), pp. 851-860 (2015). https://doi.org/10.2514/1.B35381

30. Torres-Herrera, U. and Nakamura, K. "Flow differentiation within nanotube networks with symmetric bifurcations by local bending vibration: A theoretical study", *Journal of Fluids and Structures*, **109**, 103502 (2022). https://doi.org/10.1016/j.jfluidstructs.2022.103502

31. Zhao, Y.Z., Chiu, Y.J., Yang, C.H., et al. "Research on heat-elastic coupled vibration in a rotating rigid disk rotor system", *Journal of Mechanical Science and Technology*, **36**(4), pp. 1667-1678 (2022). https://doi.org/10.1007/s12206-022-0109-7

32. Jin, Q. and Ren, Y. "Coupled resonance of FGM nanotubes transporting super-critical high-speed pulsatile flow under forced vibration: size-dependence and bifurcation topology", *Computer Methods in Applied Mechanics and Engineering*, **404**, 115834 (2023). https://doi.org/10.1016/j.cma.2022.115834

33. Zhang, W., Gu, X.J., and Zhang, Y.F. "New modeling on vibrations and bifurcations of FGGP reinforced pretwisted composite rotating blade under axial aerodynamic force: Theoretical and numerical researches", *Thin-Walled Structures*, **184**, 110523 (2023). https://doi.org/10.1016/j.tws.2023.110523

34. Luo, Z., Wang, J., Tang, R., et al. "Research on vibration performance of the nonlinear combined support-flexible rotor system", *Nonlinear Dynamics*, **98**(1), pp. 113-128 (2019). https://doi.org/10.1007/s11071-019-05176-2

35. Lv, B., Jin, X., Cao, J., et al. "Advances in numerical modeling of environmental barrier coating systems for gas turbines", *Journal of the European Ceramic*

Society, **40**(9), pp. 3363-3379 (2020). https://doi.org/10.1016/j.jeurceramsoc.2020.03.036

36. Wang, L., Wang, A., Jin, M., et al. "Nonlinear effects of induced unbalance in the rod fastening rotor-bearing system considering nonlinear contact", *Archive of Applied Mechanics*, **90**, pp. 917-943 (2020). https://doi.org/10.1007/s00419-019-01645-7

37. Liu, X. and Ma, L. "Chaotic vibration, bifurcation, stabilization and synchronization control for fractional discrete-time systems", *Applied Mathematics and Computation*, **385**, p. 125423 (2020). https://doi.org/10.1016/j.amc.2020.125423

38. Ma, L., Yao, M., Zhang, W., et al. "Bifurcation and dynamic behavior analysis of a rotating cantilever plate in subsonic airflow", *Applied Mathematics and Mechanics*, **41**, pp. 1861-1880 (2020). https://doi.org/10.1007/s10483-020-2668-8

Biographies

Youcef Mahroug received his License's and master's degrees in Mechanical Engineering, Oil field mechanics from M'hamed Bougara University Boumerdes, Algeria in 2013 and 2015 respectively. He is currently a PhD. student at Laboratory of Mechanics, Physics and Mathematical Modelling, University of Medea, Algeria. His current research interests include system identification, multivariable systems, dynamical systems theory, and stability theory of dynamical systems, vibration analysis, bifurcation and chaos Theory. His thesis aims to develop a model to identify the bifurcation behaviour of vibration of a gas turbine. He has participated in many workshops and published many national/international conferences and journals papers within his domain of interest.

Ahmed Hafaifa (Senior Member, IEEE) was born in Medjedel, Wilaya of M'Sila, Algeria in 1974, He is full Professor in Industrial Process: Automation / Reliability and Systems Diagnostics at the Faculty of Science and Technology of the University of Djelfa, Algeria. Hence, he was named permanent Dean for the Science and Technology Faculty in April 2018 until now, after serving as the leader of Science and Technology Filed for five years since October 2014. He received the Habilitation to conduct researches from the University of Sciences and Technologies Houari Boumediene - USTHB - Faculty of Electronics and Computer Science, Department of Instrumentation and Automation in 2012 and he received the PhD degree on Applied Automation and Signal Processing in 2010 and the Magister degree in 2004 on Applied Automation and control systems and the State Engineer degree in 2000 on Applied Automation from the UMBB Boumerdes University, Algeria. Currently, he is the director of the Applied Automation and industrial diagnostics Laboratory and the head of the Gas Turbines Joint Research Team, at the Faculty of Science and Technology, University of Djelfa, where he is the founder of these research entities, he initiated and supported several international research projects within the framework of collaboration and innovation activities with the industrial sector. Professor Ahmed HAFAIFA is the director of several PhD doctoral theses in Algeria and abroad and the coordinator of several industrial research projects in the field of applied automation and reliability engineering. These projects focus on development sustainable solutions in renewable energies, for sustainable energy applications as a solution of energy sustainability, to minimize the environmental impacts of these technologies, with their future trends. His research area includes modeling and control of industrial systems, engineering of reliability diagnostics and fault detection and isolation in industrial processes, sustainable renewable energy solutions, intelligent systems based on fuzzy logic and neural networks. He acts as an expert in several national and international commissions and in joint collaborative research activities. He has supervised several PhD and Masters students and published many national and international conferences and journals papers. In addition, he is a member in international research projects and he leads national research projects.

Abdelhamid Iratni (IEEE Member) is an Associate Professor of Electrical Engineering at the University of Mohamed El Bachir El Ibrahimi of Bordj Bou Arreridj (Algeria). He has been teaching and conducting research at the university since 2004. He is currently the Chair of the Scientific Committee in the Electrical Engineering Department, and he previously served as the Head of the Bachelor and Master Programs in Automatic Control from 2015 to 2018. Dr. Iratni earned his B.Sc. and M.Sc. degrees in Electrical Engineering from the University of Boumerdes, Algeria, in 1999 and 2003, respectively. He received his PhD from the University of Setif, Algeria, in 2013. His primary research areas include nonlinear filtering, estimation and control, biomedical and bioprocess engineering, automation, and the reliability of industrial systems. Dr. Iratni has published over 35 papers in esteemed international journals and conferences. He has also contributed his expertise as a visiting researcher at prominent institutions such as the University of Central Florida (USA), the University of Coimbra (Portugal), and the Institute of Systems & Robotics (Portugal). His extensive experience and contributions have solidified his position as a reputable figure in his field.

Mouloud Guemana (IEEE Member) was born in Medea, Algeria in 1975. He received the state engineer degree of the national institute of hydrocarbons and chemistry INH on Mechanical Engineering from the University of Boumerdes, Algeria, in 1998. From May 1999 to January 2003, He was associated researcher and associated lecturer. He received his Magister at the University of Boumerdes, Algeria in 2003. He received the PhD degree in Industrial Maintenance in 2012. Currently he is an associate Professor at the University of Medea, Algeria. He is the head of the reliability in industrial systems group at the Applied Automation and Industrial Diagnostic Laboratory. He is the author and co-author of many scientific papers and research projects. His research interests include industrial maintenance, reliability system, dynamical systems, and diagnostic and reliability optimization.

Ilhami Colak (Senior Member, IEEE) was born in 1962 in Turkey. He received the diploma degree in electrical engineering from Gazi University, Ankara, Turkey, in 1985, the M.Sc. degree in electrical engineering in the field of speed control of wound rotor induction machines using semiconductor devices from Gazi University, in 1991, the M.Phil. degree from Birmingham University, Birmingham, U.K., in 1991, by preparing a thesis on high-frequency resonant dc-link inverters, and the PhD degree from Aston University, Birmingham, U.K., in 1994, with a focus on mixed-frequency testing of induction machines using inverters. He became an Assistant Professor, an Associate Professor, and a Full Professor in 1995, 1999, and 2005, respectively. He was the Head of Department, Dean, and Vice Rector of Gazi University, Istanbul Gelisim University, and Nisantasi University, Istanbul, Turkey. He is currently a Full Professor with Nisantasi University. He has authored or coauthored more than 120 journal papers, 235 conference papers, and 7 books in different subjects, including electrical machines, drive systems, machine learning, reactive power compensation, inverter, converter, artificial neural networks, distance learning automation, and alternating energy sources.